AMERICAN UNIVERSITY OF BEIRUT

LOW-THRESHOLD AND CALCIUM-DEPENDENT POTASSIUM CURRENTS REGULATE THE INTRINSIC FIRING PROPERTIES OF FOREBRAIN-PROJECTING HVCRA NEURONS IN ZEBRA FINCHES

by
SALLY SAMIR CHOKER

A thesis
submitted in partial fulfillment of the requirements
for the degree of Master of Science
to the Biomedical Engineering Program
of Maroun Semaan Faculty of Engineering and Architecture
and the Faculty of Medicine
at the American University of Beirut

Beirut, Lebanon
April 2022

AMERICAN UNIVERSITY OF BEIRUT

LOW-THRESHOLD AND CALCIUM-DEPENDENT POTASSIUM CURRENTS REGULATE THE INTRINSIC FIRING PROPERTIES OF FOREBRAIN-PROJECTING HVCRA NEURONS IN ZEBRA FINCHES

by

SALLY SAMIR CHOKER

Approved by:

	Signature
Dr. Arij Daou, Assistant professor Biomedical Engineering Program	Advisor
	Signature 
Dr. Wassim Nassreddine, Associate Professor Department of Neurology	Co-Advisor
	Signature 
Dr. Rami Mhanna, Assistant professor Biomedical Engineering Program	Member of Committee
	Signature 
Dr. Fadi Karameh, Associate professor Department of Electrical and Computer Engineering	Member of Committee

Signature

Dr. Daniel Margoliash, Professor
Department of Neuroscience, University of Chicago

Member of Committee

Signature

Date of thesis defense: April 25, 2022

AMERICAN UNIVERSITY OF BEIRUT

THESIS RELEASE FORM

Student Name: ____Choker_____ Sally_____ Samir___
Last First Middle

I authorize the American University of Beirut, to: (a) reproduce hard or electronic copies of my thesis; (b) include such copies in the archives and digital repositories of the University; and (c) make freely available such copies to third parties for research or educational purposes:

☒ As of the date of submission

☐ One year from the date of submission of my thesis.

☐ Two years from the date of submission of my thesis.

☐ Three years from the date of submission of my thesis.

_____

Signature Sally Choker Date 10-5-2022

ACKNOWLEDGEMENTS

I would like to start by thanking my thesis advisor Dr. Arij Daou for his continuous support throughout my graduate studies. I had the honor to work with him on my thesis project and I highly appreciate his professionalism along with his values and morals.

I would also like to thank my thesis committee members: Dr. Rami Mhanna, Dr. Fadi Karameh, Dr. Wassim Nassreddine and Dr. Daniel Margoliash for their insightful and constructive comments.

Finally, I am sincerely grateful to my family whose love and support always motivate me to get to the better version of me. I am thankful for their care and reassurance that always helped me in overcoming obstacles and hard times I have been through throughout life. This accomplishment would not have been possible without them.

ABSTRACT
OF THE THESIS OF

Sally Samir Choker for Master of Science
Major: Biomedical Engineering

Title: Low Threshold and Calcium activated Potassium Currents Regulate the Intrinsic Firing Properties of Forebrain Projecting Neurons in Zebra Finches

Vocal control and learning are dependent on auditory feedback in both songbirds and humans, rendering songbirds as an excellent model to study the neural mechanisms of complex learned behavior. The telencephalic nucleus HVC within the songbird, analogue to the mammalian pre-motor cortex, produces stereotyped instructions through the motor pathway leading to precise, learned vocalization. The forebrain projecting HVC neurons (known as HVC_{RA}), that projects to the robust nucleus of the arcopallium, play a critical role in orchestrating the neural circuitry that guides the bird's learning and song production. Whole cell current-clamp recordings previously performed on HVC_{RA} neurons within brain slices have shown a diversity in their firing activity across birds, ranging from transient to stuttering patterns (Daou & Margoliash, under review). We developed a biophysical model that captures the diversity of the HVC_{RA} firing activity. The model generated predictions about the ionic currents that HVC_{RA} exhibit which were tested and verified in the slice using pharmacological manipulations. The model highlights important roles for the low-threshold potassium currents(I_D) and (I_M) and the Ca^{2+}-dependent K^+ current (I_{SK}) in driving the characteristic neural patterns observed in HVC_{RA}.

Methods

We used a single-compartment conductance-based Hodgkin-Huxley like biophysical model of HVC_{RA} neurons to estimate the magnitude of the ionic currents. Manual adjustment of the densities of the ionic conductances and additional parameters was performed to match the membrane potential model trajectories to the biological trace in response to applied step currents. To estimate the goodness of the fit, we adopted a feature-based comparison approach in which intrinsic features of simulated voltage traces and biological traces are compared. The model is then validated by testing the fitted model trace to predictions of different current injections.

TABLE OF CONTENTS

ILLUSTRATIONS

Figure

TABLES

Table

CHAPTER 1

INTRODUCTION

1.1 Study background

Oscine songbirds (e.g., zebra finches, canaries, and white-crowned sparrows) have been extensively used as a model system to study complex learned behavior. The song produced by a songbird is learned in much the same way that humans acquire several motor skills, and more specifically speech learning (Bolhuis, Okanoya, and Scharff 2010b; Brainard and Doupe 2002, 2013). Birdsong learning shares strong parallels with speech acquisition. Like humans, birds must hear the sounds of adults during an early sensitive period and also must hear their own voice while learning to vocalize (Doupe and Kuhl 1998a). Songbirds thus provide a promising model system for elucidating general neural mechanisms involved in vocal learning, both in normal states and disease.

Birdsong is driven by a discrete set of well-characterized premotor brain nuclei specialized for song learning and production, known as the 'song system'.(this system is described in detail in 0, 2.3 Neural substrates for vocal learning: song control circuits) (Mooney 2009). Among these structures, the telencephalic nucleus HVC (proper name), analogous to the mammalian pre-motor cortex, is known to have a central role in controlling the temporal structure of the song (**Figure 1**-a). During singing, each neuron in HVC projecting to downstream premotor nucleus RA (robust nucleus of the arcopallium) emits only a single highly stereotyped burst of several spikes during each repetition of the song

motif (**Figure 1**-b) (Hahnloser, Kozhevnikov, and Fee 2002a). A motif is a sequence of smaller vocal gestures, called syllables, occurring repeatedly. This burst sequence drives activity in RA, which in turn drives the motor neurons that control vocalization. Thus, the RA-projecting neurons, denoted as 'HVC_{RA}', are of prime importance for singing, innervating the motor neurons essential for song production. However, the circuit and cellular mechanisms in HVC responsible for HVC_{RA}'s sparse pattern of activity remain an active area of research. Numerous intracellular and extracellular recording studies of HVC neurons have been carried out and models to investigate HVC's internal circuitry have been proposed. These studies revealed a variety of physiological properties within the HVC. However, the cellular activity of HVC_{RA} neural population remained poorly characterized.

1.2 Study aims

In this study, we aim to investigate the ionic mechanisms underlying the HVC_{RA} firing pattern among a particular species of songbirds, the zebra finches. Whole cell current-clamp recordings which were previously performed on HVC_{RA} neurons within brain slices have shown diversity in their firing activity, ranging from transient to stuttering patterns (**Figure 2**) (Daou & Margoliash, under review). A previous work by Arij Daou and his co-workers (Daou et al. 2013), found that a calcium-activated apamin sensitive potassium current (I_{SK}) contributes to the phasic firing of HVC_{RA}. However, the ionic basis behind the rest of the firing patterns remained unknown.

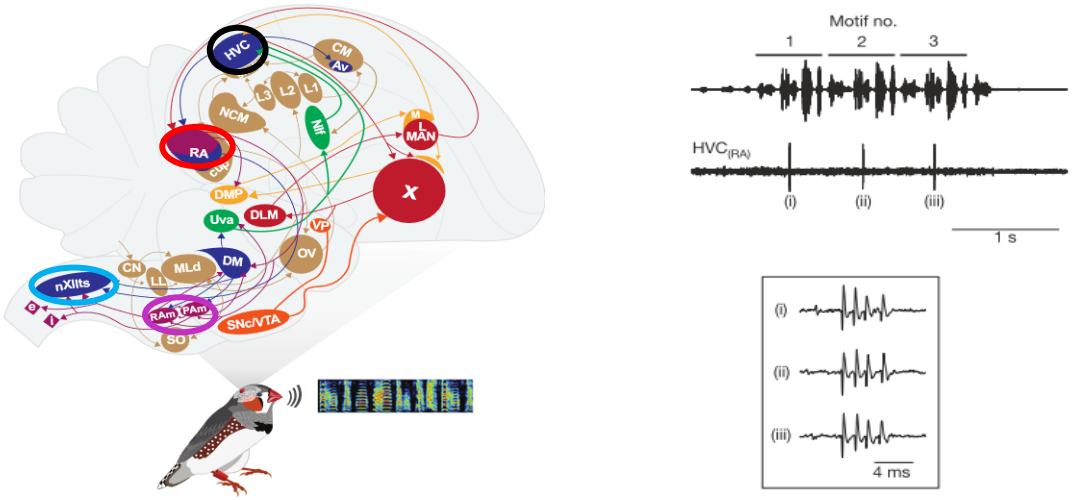

Figure 1 (a) Schematic of a male zebra finch along with a sample spectrogram of a song (bottom). Avian brain nuclei related to song control (top). The vocal organs are innervated by motor neurons in the brainstem (nXIIts, circled in blue). Nucleus retroambigualis (RAm), nucleus parambigualis (PAm) (circled in purple) and nucleus nXIIts, responsible for vocal production, are innervated by forebrain nucleus RA (circled in red). Nucleus RA is innervated by projection neurons (HVC_{RA}) within nucleus HVC (circled in black). (Adopted from (Daou and Margoliash 2021)). (b) Extracellular recording of a single HVCRA neuron (bottom), with the simultaneously recorded vocalization (top). The HVCRA neuron generates a single burst of spikes during each repitition of the song motif (Hahnloser et al. 2002a)

What ion channels could be responsible for these spiking behaviors? Does this heterogeneity in firing implicate the classification of HVC_{RA} neurons into different types? We advance two hypotheses.

1. We hypothesize the expression of two low threshold potassium currents in HVC_{RA}, the slowly inactivating K^+ current I_D, and the non-inactivating K^+

current I_M. The collective activity of I_M, I_D and I_{SK} accounts for the diverse evoked responses of HVC_{RA}.

2. We propose the classification of HVC_{RA} neurons into three types based on the ion channels mainly governing the firing behavior. Type I encompasses the cells in which I_M along with I_{SK} control the spike train, type II comprises the neurons where I_D and I_{SK} regulate the firing discharge, and type III comprises the neurons where I_D, I_M and I_{SK} drive the firing activity.

To test our hypotheses, we have developed a biophysical model that replicates HVC_{RA}'s diverse spiking patterns and generates predictions about the ionic currents present. The model highlights the important roles of I_M, I_D, and I_{SK} in driving the characteristic neural patterns. These predictions were confirmed in slice using pharmacological manipulations.

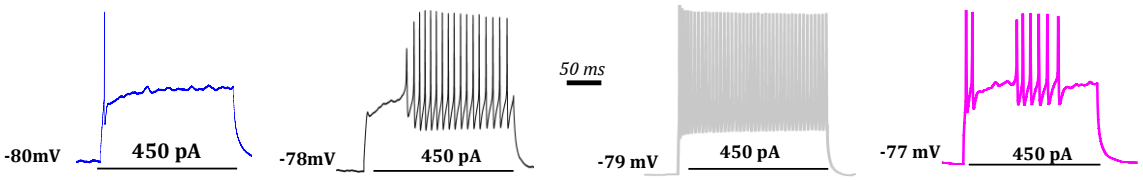

Figure 2 Current clamp recordings of four HVC_{RA} neurons (one recording/neuron) in response to a 450 pA current pulse (Daou and Margoliash, under review). Starting from left to right, the first neruon fires a single spike (phasic pattern), the following exhibits a long delay to the first spike during which the membrane voltage slowly depolarizes. The third neuron responds in a tonic pattern, the forth neuron fires 2 bursts of spikes seperated by a pause (stuttering)

CHAPTER 2

LITERATURE REVIEW

This chapter provides a summary of the basic discoveries made by studying songbirds and reviews the roles of specific ion channels in generating different firing patterns. We present first the behavioral parallels between birdsong and human speech. We describe next the process of vocal learning and the neural sub-states essential for song acquisition and production. In the following sections, we highlight the neural activity of one of the most studied nuclei essential for song production, nucleus HVC, with an emphasis on the HVC_{RA} neural population (neurons of interest in our study). We describe the electrophysiological activity of HVC_{RA} *in vivo* and *in vitro*. We highlight next the similarities of HVC_{RA}'s spiking activity with the firing behavior of the mammalian central neurons. We detail then how the expression of particular channel types underlies the generation of characteristic patterns of various types of neurons. Finally, we present the previous models of HVC_{RA} and discuss their limitations.

2.1 Why study songbirds

Vocal learning is the ability to modify the acoustic and/or syntactic structure of sounds produced, including imitation and improvisation (Jarvis 2007). It is also a crucial factor for speech acquisition. Humans are excellent vocal learners as they have the ability to imitate speech sounds that they hear and modify them through auditory feedback. However,

vocal learning among non-human species is quite rare. Among mammals, only cetaceans (whales and dolphins), elephants, and some bats show evidence of vocal learning. In contrast, many thousands of songbird species, as well as of parrots and hummingbirds, share the capacity of vocal learning with humans (Brainard and Doupe 2002; Doupe and Kuhl 1998b). Songbirds share numerous parallels to human speech learning, therefore, represent a unique animal model to investigate mechanistically both vocal learning and its disorders.

2.1.1 Birdsong and human speech

There are notable parallels in song learning among songbirds and human speech (Bolhuis, Okanoya, and Scharff 2010a; Doupe and Kuhl 1998a). First, both humans and songbirds must be able to hear others and themselves to develop normal vocalization. Birds do not learn to sing normally, nor infants to speak, if they are not exposed to the communicative signals of adults of their species. Profound speech deterioration manifests in children if they become deaf early or late in childhood (Cowie and Douglas-Cowie 1992). Second, in both humans, and songbirds, there is a critical period occurring early in development when auditory–vocal learning is accomplished best, called the 'sensory' learning phase (**Figure 3**). This early phase of learning is primarily perceptual and serves to guide later vocal production. In humans, the ability to learn new languages without formal instruction is decreased after puberty. Finally, in both species, the 'sensory' (listening) phase precedes a production or a 'sensorimotor' phase. The sensorimotor phase begins once infants begin to 'babble'- or juvenile birds produce song-like sounds denoted as the 'subsong'. During this phase, both infants and juvenile birds practice their own vocalizations and try to

match them to the learned perceptual target using auditory feedback (Bolhuis et al. 2010a; Doupe and Kuhl 1998b; Mooney 2009).

However, birdsongs are not homologous to human language: birdsong is not similar to language in the sense of conveying complex meaning. It also lacks the rich structure and semantics of the human language. Birdsong may be more analogous to speech which refers to the ability to produce learned vocalizations exhibiting semantic content (Brainard and Doupe 2002; Doupe and Kuhl 1998b). Despite these differences, the striking similarities that birdsong learning shares with human speech acquisition render birdsong as a great model system to investigate complex learned behavior.

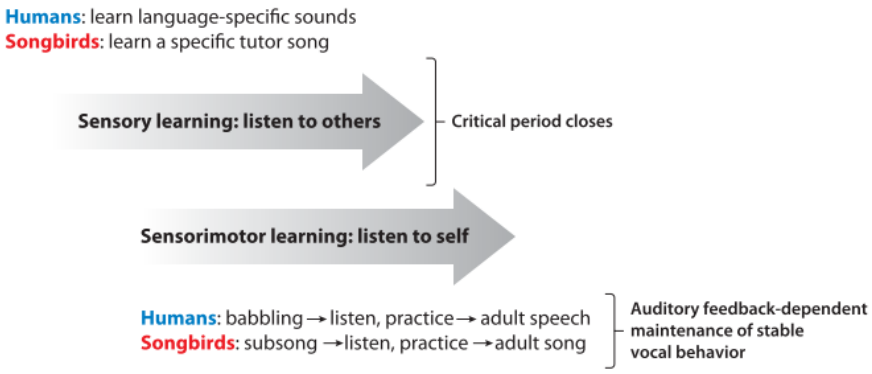

Figure 3: Similarities between birdsong and human speech. In both humans, and songbirds, there is an early critical 'sensory' learning phase during which infants and juvenile birds listen to the sounds of others. This phase is followed by a 'sensorimotor' phase during which infants and juvenile birds practice their own vocalizations and try to match them to the memorized targets using auditory feedback. Figure extracted from (Brainard and Doupe 2013)

2.1.2 Zebra finches: an avian model for vocal learning

One songbird, in particular, the zebra finch (Taeniopygia guttata) has been the focus of much research because of its prolific breeding and rapid maturation (**Figure 4**). Only male zebra finches have the capacity to learn and sing, while female zebra finches do not sing. This has been related to the reason that male zebra finches have an elaborate network of forebrain nuclei known as the "song system", while female zebra finches do not exhibit this system (Mooney 2009).

Figure 4 Female (left) and male (right) zebra finches. Male zebra fiches have orange cheek patches, black bar on the breast and a chestnut-colored flank with white spots, while females lack these features. Beak color is red in males and orange in females.

The male zebra finch adult songs are highly stereotyped throughout their lives, making them well suited for in-depth analysis. The song of an adult male zebra finch song consists of a few short introductory notes (the simplest individual sounds that birds produce), followed by several repetitions of motifs, separated by brief periods of silence (**Figure 5**). A

motif is a stereotyped sequence of syllables and a syllable consists of one or more notes occurring together(Berwick et al. 2011; Brenowitz, Margoliash, and Nordeen 1997).

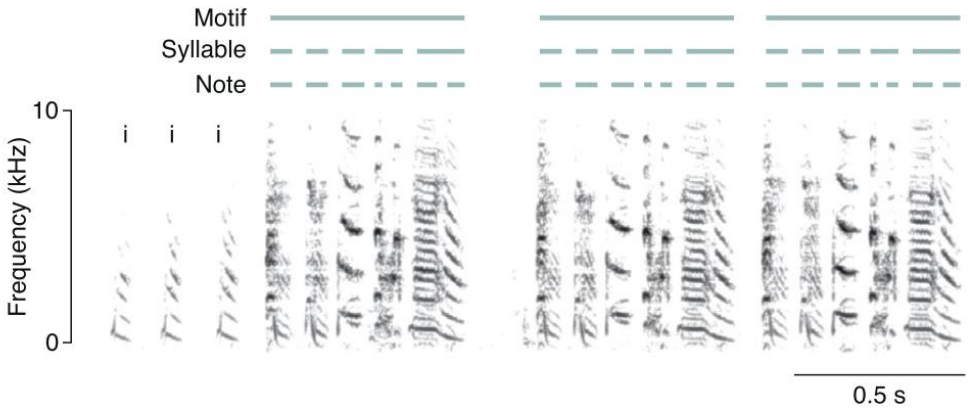

Figure 5 Song spectrogram of a zebra finch. Sound energy is plotted as a function of frequency and time. The intensity of the sounds is represented by grayscale. Songs start with introductory notes (denoted by 'i') that are followed by one or more motifs. A repeated sequence of syllables is called a motif. A syllable consists of one or more notes occurring together. (from (Berwick et al. 2011))

2.2 Process of vocal learning

The song learning process in songbirds occurs in two distinct stages: sensory learning and sensorimotor learning phases (**Figure 6**) (Mooney 2009). During the sensory learning phase, the juvenile songbird listens to and memorizes the song of an adult tutor male (oftentimes its father or an adult male conspecific). The memorized song is called the 'template'. During the sensorimotor learning phase, the juvenile begins to practice his own vocalizations and matches his song to the memorized template using auditory feedback.

Sensorimotor learning is comprised of three stages: the subsong, plastic song, and crystallized song. In the beginning, the juvenile produces highly variable vocalizations known as the 'subsong'; this stage is homologous to the babbling of human infants. With further vocal practice, the subsong gradually evolves to a more structured but still variable song called the plastic song. The plastic song is progressively refined until the bird produces crystallized songs where the variability is substantially eliminated and the song exhibits a strong resemblance to the tutor song (Fee and Scharff 2010). The crystallized song serves to attract females and defend territory from other males.

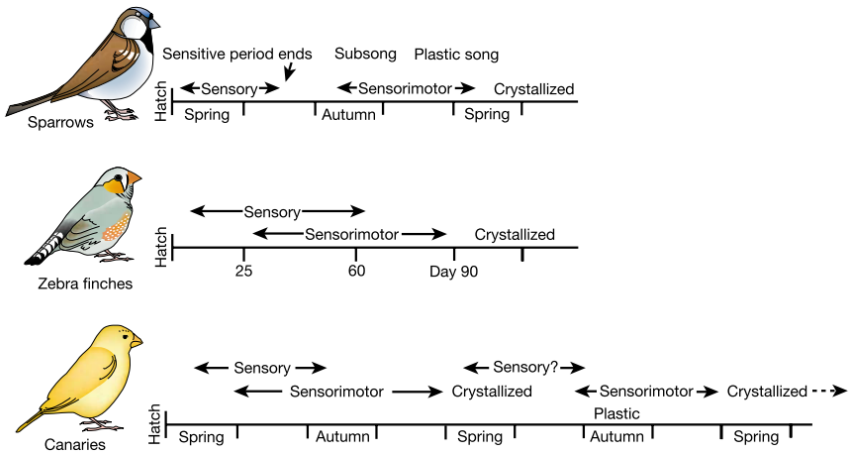

Figure 6 Developmental timeline of song learning. In white crown sparrows, the sensory and sensorimotor phase are separated by many months (top), while in zebra finches, the two phases overlap extensively (middle). Canaries, classified as open learners can continue their song learning process beyond their first year (bottom) (from(Brainard and Doupe 2002)).

The developmental timeline for song learning differs among species of songbirds (**Figure 6**). In zebra finches, the sensory and sensorimotor phases overlap extensively, and the song is crystallized between 90- and 120-days post-hatch (dph). While in white-crown sparrows, the sensory and sensorimotor phases are separated in time and song crystallization occurs at the end of the first year of the bird's life (Mooney 2009). Zebra finches and white-crowned sparrows are classified as 'age-limited learners', as they learn only during their first year of age. On the other hand, 'open learners' such as the canaries, may develop new song patterns beyond their first year of life, generally in a seasonal manner (Brenowitz et al. 1997)

2.3 Neural substrates for vocal learning: song control circuits

A specialized network of interconnected forebrain nuclei, essential for song learning and production, distinguishes the brain of songbirds from the brain of birds that do not learn to vocalize. (Brenowitz et al. 1997; Kozhevnikov and Fee 2007; Mooney 2009). This particular neural circuitry is known as the 'song system'. Two major pathways of the song system are involved in song learning and production: the vocal motor pathway (VMP), necessary for the production and acquisition of a learned song, and the anterior forebrain pathway (AFP), necessary for song recognition and acquisition (**Figure 7**). The telencephalic song nucleus higher vocal center (HVC). is at the starting point of both VMP and AFP. However, these two pathways arise from two different populations of HVC projection neurons. The VMP receives premotor input from one subset of HVC projection neurons, referred to as 'HVC_{RA}'. These neurons project to the robust nucleus of the archistriatum (RA) which controls the vocal and respiratory neurons used for singing. RA nucleus contains

projection neurons that innervate the tracheosyringeal portion of the nucleus hypoglossus (nXIIts) and the respiratory premotor neurons. The respiratory premotor neurons encompass the nucleus retroambigualis (RAm) and the nucleus parambigualis (PAm), which control, respectively, expiration and inspiration during singing (Wild 1993). The neurons of nXIIts in their turn innervate the syrinx, the muscles that are responsible for generating vocal output. Thus, nucleus RA drives the motor neurons responsible for vocalization. HVC in its turn receives input from the thalamic nucleus uvaeformis (Uva).

The anterior forebrain pathway receives auditory input from a distinct subset of HVC projection neurons, denoted as HVC_X. HVC_X neurons project to Area X, the basal ganglia analog in songbirds, which in turn innervates the thalamic nucleus DLM. The thalamic nucleus DLM projects then to the anterior telencephalic nucleus (LMAN) which in turn innervates nucleus RA, providing it with auditory input. Additionally, LMAN projects to area X, hence offering the potential for feedback within this pathway. Thus, the AFP indirectly connects HVC to RA via the thalamic nucleus DLM and the anterior telencephalic nucleus LMAN (Brenowitz et al. 1997)

To understand the neural mechanisms underlying song learning and production, it is critical to characterize the activity of its interconnected forebrain nuclei essential for singing and acquisition. Because of the crucial importance of HVC for song production (Kozhevnikov and Fee 2007), it is one of the most studied nuclei in the song system. HVC neural types and their patterns of activity *in vivo* and *in vitro* have been well characterized (Daou et al. 2013; Daou and Margoliash 2020; Dutar, Vu, and Perkel 1998; Kozhevnikov

and Fee 2007; Kubota and Taniguchi 1998; Mooney 2000; Mooney and Prather 2005) and will be summarized in the following section.

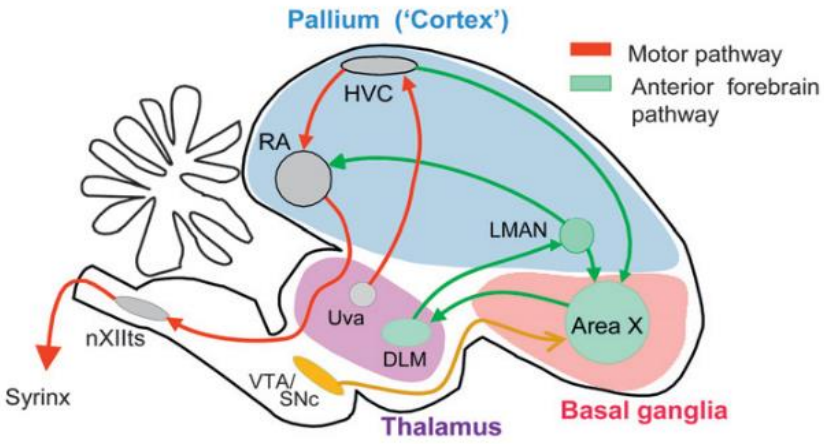

Figure 7 Simplified diagram of song system illustrating the songbird brain with projections of major nuclei. The VMP (red arrows) is responsible for song production and the AFP is essential for song learning (green arrows). In the VMP, the syrinx is innervated by motor neurons in the brainstem (nxIIts), which receives input from nucleus RA. Nucleus RA receives premotor input from HVC, which is innervated by thalamic nucleus Uva. The AFP consists of nucleus HVC which sends auditory input to Area X. Area X in turn innervates the thalamic nucleus DLM. which projects to the anterior telencephalic nucleus (LMAN). LMAN in turn innervates nucleus RA and area X. (from (Fee and Scharff 2010)).

2.4 The telencephalic song nucleus HVC

HVC exhibits singing-related activity. Neurons in HVC emit precise premotor activity when the bird is singing (Hahnloser et al. 2002a; Yu and Margoliash 1996). Early electrophysiological experiments suggest that this singing-related activity propagates down

the VMP, arising earlier in HVC than in RA. HVC is responsible for generating the syllable order and tempo of the song while nucleus RA represents individual syllables (Vu, Mazurek, and Kuo 1994). Furthermore, HVC may be a site for encoding the tutor's song in the brain. A study by Todd Roberts and his colleagues found that electrical disruption of neural activity of the telencephalic nucleus HVC of juvenile zebra finches, as they listen to the tutor's song, prevented song copying, consequently, producing poor copies of the tutor's song (Roberts et al. 2012).

HVC is structurally heterogeneous, comprised of at least three major types including two relay cell types and interneurons. One type of projection neurons (HVC_X) innervates area X within the anterior forebrain pathway (AFP) essential for song learning and perception. The other type of projection neurons (HVC_{RA}) innervates area RA, which drives the motor neurons controlling vocalization. HVC_X, HVC_{RA}, and interneurons (HVCint) are distinguished from each other based on their morphology and their intrinsic electrophysiological properties (Daou et al. 2013; Mooney 2000; Mooney and Prather 2005).

2.4.1 Morphological identification of HVC neural types

Intracellular staining of HVC neurons with biocytin or neurobiotin allows to morphologically identify the three distinct classes. HVC projection neurons and interneurons can be differentiated anatomically by their dendritic extent, their projecting axons, and the size of their soma (Mooney 2000; Mooney and Prather 2005). HVC_{RA} neurons are characterized by sparsely spinous dendrites and a main axon that projects caudally to nucleus RA. HVC_X neurons, on the other hand, possess thicker and more spinous dendrites, with

their main axon projecting rostrally to area X. HVCint are characterized by aspinous varicose dendrites, and their processes are entirely restricted to HVC. Additionally, X-projecting neurons possess larger cell bodies than HVC_{RA} and HVCint, while HVC_{RA} neurons have a smaller soma compared to HVCint (**Figure 8**).

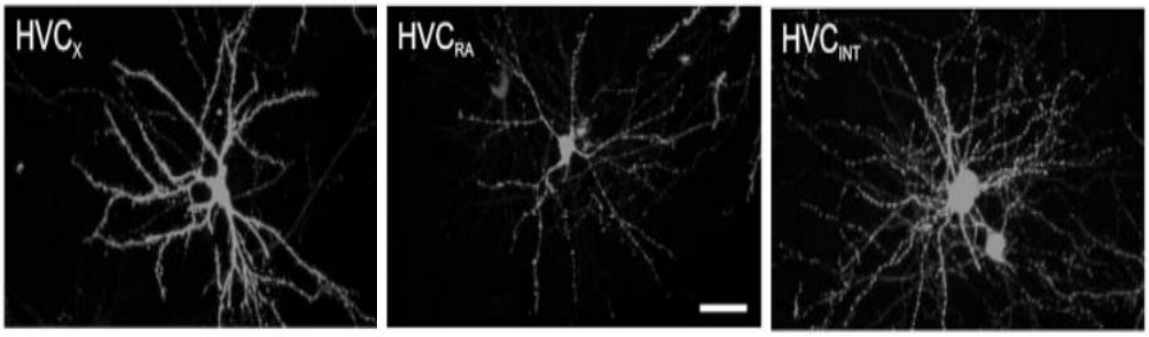

Figure 8 Morphological identification of HVC neuron types. HVCx are characterized with thicker and more spinous dendrites than HVC_{RA} (middle), which possess slender and sparsely spinous dendrites. HVCint have aspinous varicose dendrite. HVC_{RA} possess a small soma compared to HVCx and HVCint and HVCx have the largest cell bodies.(from (Mooney and Prather 2005)).

2.4.2 Electrophysiological identification of HVC neural types

Previous *in vitro* studies indicated that different morphological classes of HVC neurons in adult male zebra finches possess distinct intrinsic electrophysiological properties (Daou et al. 2013; Dutar et al. 1998). The three classes of HVC neurons are differentiated according to their DC evoked firing responses *in vitro* (Figure 9). In response to a hyperpolarizing pulse, HVC_X show a fast and time-dependent inward rectification with a little sag, followed by moderate rebound firing on the termination of the pulse (**Figure 9**- a).

HVCint, on the other hand, present a prominent sag accompanied by a strong rebound firing at the end of the negative current pulse (**Figure 9**-c), while HVC_{RA} display no sag at all (**Figure 9**-b).

In response to depolarizing current pulses, HVCint are distinguished from the two relay cell types by their high frequency, non-adapting action potentials (**Figure 9** c). HVC_X, on the other hand, fire in a regular pattern with spike frequency adaptation (a time-dependent decrease in action potential discharge rate) when injected with a depolarizing current pulse (**Figure 9**-a). Unlike HVC_X and HVCint, RA-projecting neurons (HVC_{RA}) are characterized by their lack of excitability and often delayed response (**Figure 9**-b) (Daou et al. 2013). These neurons exhibit diversity in their firing activity ranging from phasic to stuttering patterns.

2.5 Characterization of HVC_{RA} activity

2.5.1 In vivo response

Extracellular (Hahnloser, Kozhevnikov, and Fee 2002b; Kozhevnikov and Fee 2007; Mooney 2000) and intracellular (Long, Jin, and Fee 2010) recordings of RA-projecting neurons in singing zebra finches have shown that this neural population displays temporally sparse, precise, and stereotyped activity. Individual HVC_{RA} neurons emit only a single brief burst (6-10 msec) of action potentials during the entire ~1s motif (**Figure 10**). Each burst of an individual HVC_{RA} neuron is generated at precisely the same time point (referenced to an acoustic landmark in the motif) during repeated renditions of the motif (Hahnloser et al.

2002b)(**Figure 11**). It has been suggested that this precise and sparse activity serves to specify the timing of syllables, notes, and even the intervening gap between syllables (Mooney 2009). Some HVC_{RA} neurons burst during these silent gaps consistent with this idea.

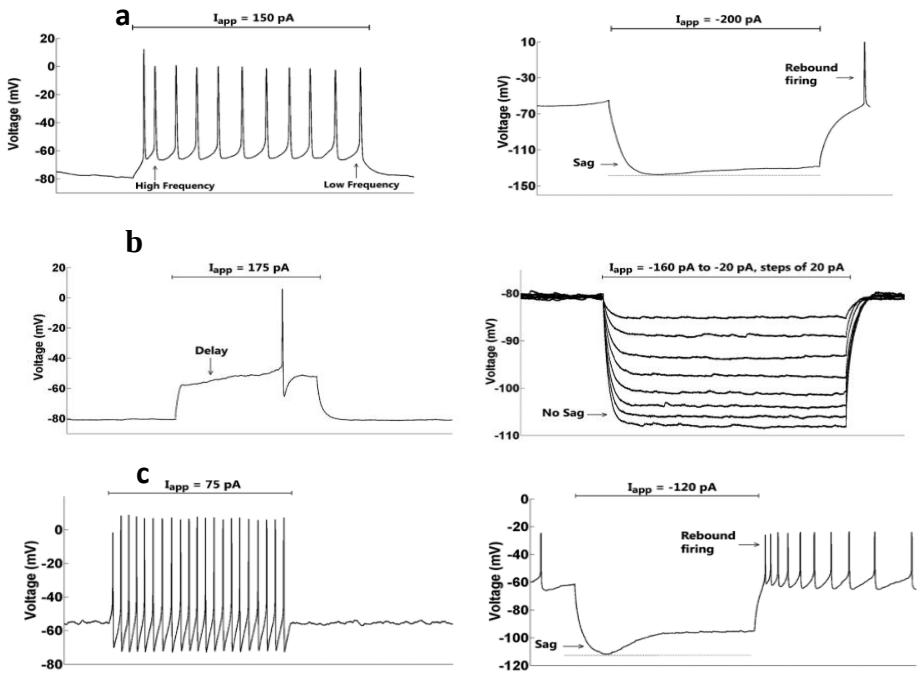

Figure 9 Electrophysiological identification of HVC neuron types. In response to a depolarizing current pulses (left column), (a) HVC_X fires tonically with SFA, (b) HVC_{RA} fires a single spike often with a delay (c) HVCint exhibits high frequency firing with no adaptation. In response to hyperpolarizing pulses (right column), (a) HVC_X exhibit little sag with moderate rebound firing, while (c) HVCint exhibit more prominent sag followed by a strong rebound firing, and HVCRA shows no sag (b). From (Daou et al. 2013).

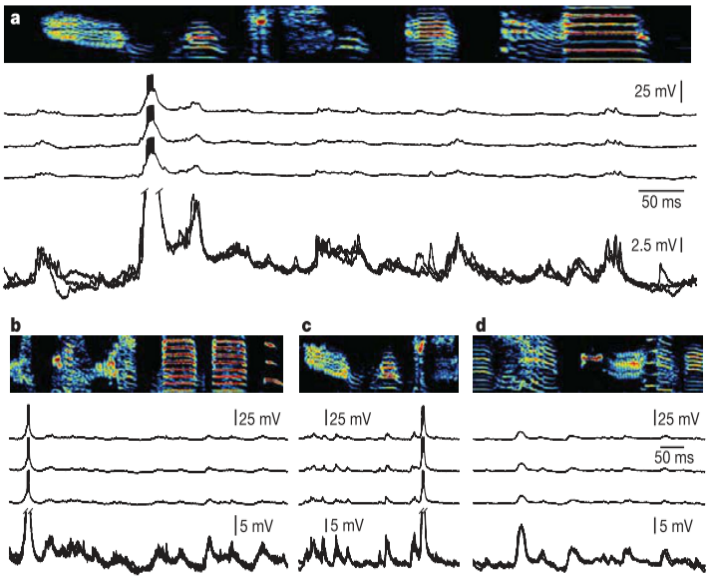

Figure 10 Intracellular membrane potential of four HVC_{RA} neurons during singing. For each cell, activity from three motif renditions is shown aligned to the song (top). An overlay of the membrane potential traces expanded is shown in the bottom of each panel(a-d). HVC_{RA} neurons in panels a,b and c generated a single burst during each song motif. HVC_{RA} neurons in (d) did not spike during song motifs. From (Long et al. 2010).

Based on the observation that different HVC_{RA} neurons burst once at different time points in the song, it has been hypothesized that these neurons generate a continuous sequence of activity over time (Fee and Scharff 2010). In other words, the bursting activity of HVC_{RA} propagates through synaptically connected HVC_{RA} neurons, like a series of falling dominoes, creating a timing signal that spans the entire song motif (**Figure 12**). Hence, song timing is controlled by the propagation of activity through a chain of RA-projecting neurons in HVC.

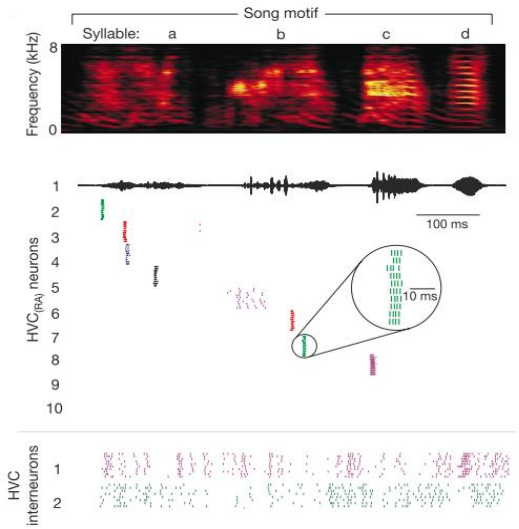

Figure 11 Spike raster plot of 10 HVC_{RA} neurons and two HVCint recorded in a single singing zebra finch. Each row of tick marks shows spikes generated during one rendition of the song. Ten renditions are shown for each neuron. Each neuron generates exactly one burst of ~6 ms duration during each rendition of the song motif. HVC_{RA} neurons burst reliably at a single precise time in the song while, HVC interneurons burst densely throughout the song (Hahnloser et al. 2002b) .

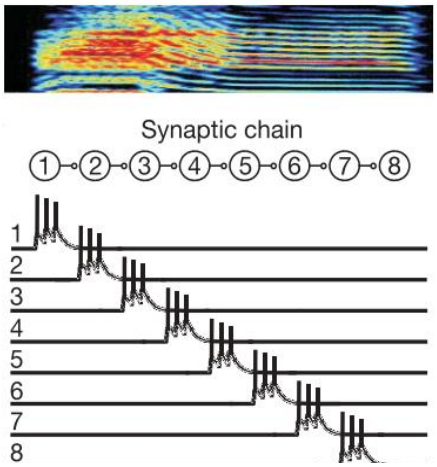

Figure 12 Activity through HVC propagates like a chain of falling dominoes. Neurons might form a synaptically connected chain such that the activity propagates from one group neurons to the next (figure from (Long et al. 2010)

2.5.2 In vitro responses

Whole cell current-clamp recordings previously performed on HVC_{RA} neurons, at the University of Chicago, show diversity in their firing activity ranging from phasic to stuttering patterns. Responses from four HVC_{RA} neurons of four birds are displayed (1neuron/bird) in **Figure 13**. Each HVC_{RA} neuron is injected with increasing magnitudes of depolarizing currents.

The response of HVC_{RA} neurons to current pulses of increasing magnitudes tended to show systematic variation. The firing pattern of HVC_{RA} of Bird 1, labeled as Orange 224, is characterized by (1) a phasic behavior or a single spike in response to the rheobase (a rheobase is the minimal current magnitude required to initiate a spike), (2) slow increase in membrane voltage (ramp) following the initial spikes, (3) a tonic evoked firing response to higher magnitude of current pulses, and (4) a sudden increase in the firing rate in response to increasing magnitudes of injected current. In contrast, the spiking pattern of HVC_{RA} neuron of Bird 2, Orange 228, is characterized by (1) a phasic evoked response to the rheobase, (2) a transient firing activity in response to higher magnitudes of current pulses, and (3) a progressive increase in the firing rate in response to increasing magnitudes of injected current. Similarly, HVC_{RA} neuron of Bird 3, Lilac 104 responded in a phasic pattern to the rheobase and exhibited a progressive increase in firing rate in response to increasing magnitudes of depolarizing pulses, however, in response to higher magnitudes of injected current, the cell fired in a sustained (tonic) manner with spike frequency adaptation. (spike frequency adaptation is a time dependent decrease in action potential discharge rate). We must note that in Birds 2 and 3, the membrane voltage following the initial spike tends to

stabilize rather than slowly increasing with time in the case of Bird 1. At last, the spiking pattern of HVC_{RA} neuron of Bird 4, labeled as Orange 112, differed from the other three cells with its delayed and stuttering response to different magnitudes of current pulses. HVC_{RA} neuron of bird 4 in response to the rheobase displayed a long delay to spike during which the membrane voltage slowly depolarizes, followed by a sustained train of spikes. When higher current pulses were injected, a stuttering (STUT) discharge was induced. The stuttering discharge is described as the occurrence of 2 or multiple bursts of action potentials separated by a pause.

To summarize, in response to the rheobase, the HVC_{RA} spiking pattern is characterized by either (1) a phasic firing followed by slow membrane depolarization, (2) a phasic firing followed by stabilization of the membrane potential, or (3) a delayed response. When a higher magnitude of the current is injected, it either fires (1) tonically with no SFA, (2) transiently, (3) tonically with SFA, or (4) in a stuttering pattern.

2.6 Similarity of activity with mammalian central neurons

The diverse firing activity of HVC_{RA} neurons in response to depolarizing current is homologous to the spiking pattern of numerous types of mammalian central of neurons (Simon P Aiken, Lampe, and Brown 1995; Rothman and Manis 2003; Shu et al. 2007; Storm 1988; Toledo-Rodriguez et al. 2004). Axons of layer 5 of rat pyramidal neurons fire phasically in response to axonal current injections The single spike is followed by a slow depolarizing ramp of the axonal membrane potential (**Figure 14** a) (Shu et al. 2007). This

characteristic firing activity was shown to be dependent on a slowly inactivating dendrotoxin (DTX) sensitive potassium current. Bath application of DTX reduced the axonal spike threshold, blocked the slow depolarizing ramp, and converted the response from a single spike to a train of spikes. DTX selectively blocks potassium channels that contain either Kv1.1, 1.2, or 1.6 subunits. Thus, the slowly inactivating DTX sensitive potassium current is mediated by the Kv1 channels expressed in axonal pyramidal neurons.

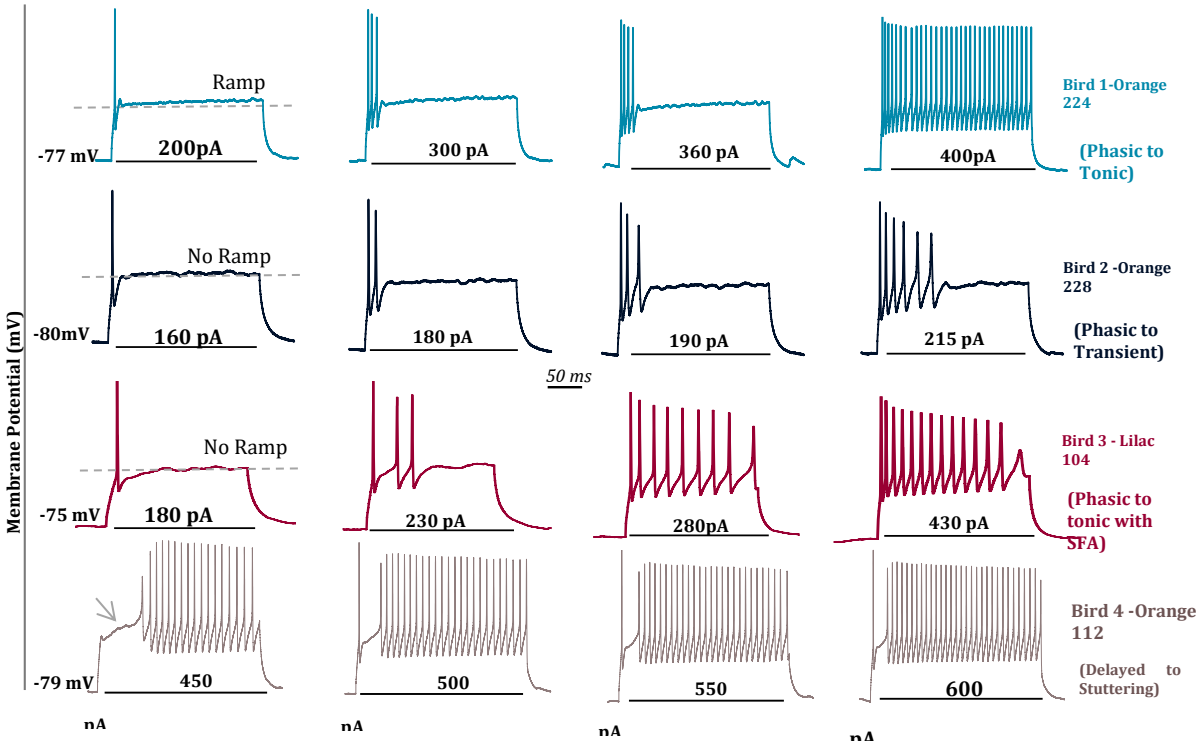

Figure 13 Whole-cell intracellular recordings from four HVC_{RA} neurons of four birds are displayed (1 neuron/bird). Each HVC_{RA} neuron is injected with increasing magnitudes of depolarizing currents (left to right). In response to the rheobase HVC_{RA} either fire a single spike followed by a slow depolarization ramp (Bird 1), or phasically with no ramp (Birds 2 and 3) or with a delay (Bird 4). In response to high magnitudes of depolarizing current, HVC_{RA} either fire tonically with no adaptation (Bird 1), or with SFA (spike frequency adaptation, a time dependent decrease in firing rate) (Bird 3), transiently (Bird 2), or in stuttering pattern (Bird 4)

Additionally, Kv1 channels are found to be correlated with the irregular spiking (stuttering) activity of neurons of the rat neocortex (Toledo-Rodriguez et al. 2004). Bath application of DTX blocked stuttering and allowed tonic spiking (**Figure 14**b). Consistent with this finding, Kv1 channels are shown to be involved in the irregular spiking of the GABAergic interneurons in the rat neocortex (Porter et al. 1998). In response to depolarizing current injections, these neurons fire a burst of action potentials followed by spikes emitted at an irregular frequency. Bath application of DTX converted this irregular pattern to a sustained mode of discharge in response to a depolarizing stimulus.

Furthermore, the slowly inactivating DTX-sensitive potassium current was shown to cause delayed excitation in rat hippocampal neurons in response to long depolarizing pulses (Giglio and Storm 2014; Storm 1988, 1990). Hippocampal neurons exhibit a long delay to the first action potential, during which the cell depolarizes slowly, in a ramp-like way. Bath application of DTX eliminated the slow ramp-like depolarization along with the long delay. Similarly, motor spinal neurons, in response to the rheobase exhibit a delayed response, during which the membrane potential slowly depolarizes (**Figure 14** c) (Bos et al. 2018). This delayed firing was also proven to be controlled by a slowly inactivating DTX sensitive potassium current, mediated by the Kv1 channels, and more specifically, the Kv1.2 subunit. Bath application of DTX and tityustoxin (TsTX), which is a selective blocker of the Kv1.2 channel subunit, prevented the slow membrane depolarization as well as the delay in onset of firing.

Therefore, the slow membrane depolarization, phasic, delayed, and stuttering patterns observed in different types of neurons are all attributed to the expression of a slowly

inactivating DTX sensitive potassium current, labeled as 'I_D' (the delay current). However, the phasic phenotype was not only associated with the expression of the Kv1 family. Rat sympathetic neurons only fire one (or a very few) action potentials in response to long depolarizing steps (**Figure 15** a). The phasic excitability was shown to be dependent on the presence of the slow voltage-gated 'M-current (I_M)' mediated by the Kv7 channel. Channel blockade with XE991 or linopirdine (selective blockers of the Kv7 channel) converted the neuron from phasic to tonic firing (Brown and Passmore 2009; Zaika et al. 2006). Similarly, I_M is present in Ca1 pyramidal neurons, and it serves to suppress repetitive firing (Simon P Aiken et al. 1995; Brown and Passmore 2009).

Thus, neuronal excitability can be strongly inhibited by the presence of Kv1 or Kv7 channels or even the co-expression of both channels. In rat vestibular cells, these two channels co-exist and serve to suppress repetitive firing discharge. Application of DTX and linopirdine converted step evoked firing patterns from phasic to sustained (Kalluri, Xue, and Eatock 2019).

I_M was not only implicated in the inhibition of repetitive firing, it may produce spike frequency adaptation (SFA), during which the firing rate is reduced during maintained depolarization (Simon P Aiken et al. 1995; Storm 1990). An additional apamin-sensitive calcium-activated potassium current (I_{SK}) may also contribute to SFA. In sympathetic neurons both currents are present, and the full tonic-firing capacity of these neurons is only revealed when both currents are blocked (Brown and Passmore 2009). Similarly, in dentate granule cells, SK and Kv7 channels coexist and regulate the neuron's firing pattern. In these cells, SK channels are the main contributors to the early spike frequency adaptation while

Kv7 channels serve to reduce firing by decreasing the spike frequency uniformly throughout the spike train (**Figure 15** b) (Mateos-Aparicio, Murphy, and Storm 2014). SK channels are also expressed in HVC_{RA} cells and they serve to suppress firing and cause SFA (Daou et al. 2013).

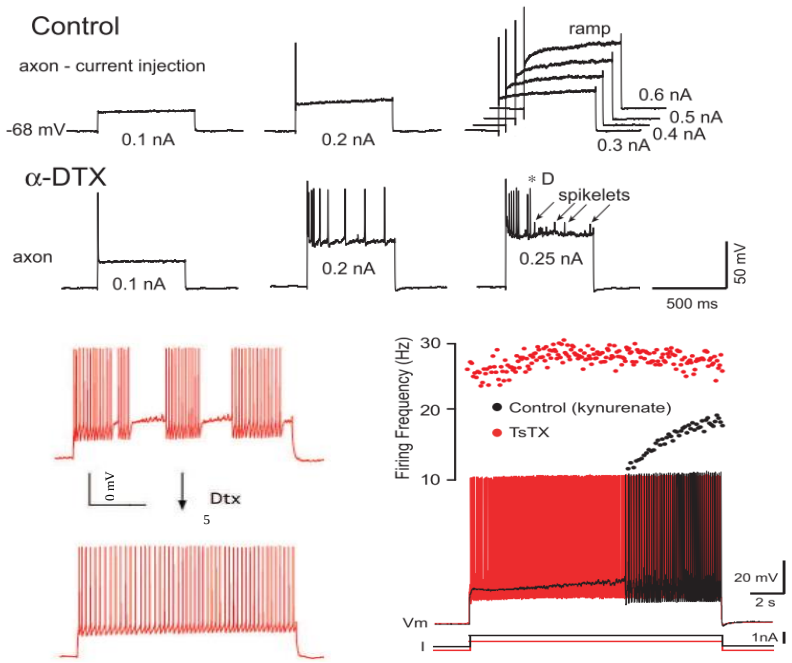

Figure 14 A low threshold slowly inactivating K^+ current accounts for the phasic, stuttering, and delayed firing. (a) Axonal injection of current pulses in rat cortical layer 5 pyramidal cells results in a single spike in the axon, followed by a slow ramping depolarization (top). After bath application of DTX, axonal spike threshold is lower, a train of spikes was generated with higher amplitude current pulses and the slow depolarizing ramp was blocked (bottom) (Shu et al. 2007). (b) Bath application of DTX in neurons of the rat neocortex blocked stuttering and allowed tonic spiking (Toledo-Rodriguez et al. 2004). (c) Bath application of TsTX converted the delayed firing response of rat motor spinal neurons to tonic discharge (Bos et al. 2018).

In summation, the neuronal intrinsic excitability of mammalian central neurons is dependent on the expression of a rich repertoire of ionic currents (Bean 2007). Specifically, I_{SK}, I_D, and I_M allow the neuron to fire with characteristic patterns (phasic, delayed, STUT, SFA) homologous to HVC_{RA}'s firing response. This similarity in firing may suggest a resemblance in the underlying ionic mechanism regulating the spiking activity, which implicates the potential expression of the delay current (I_D) and M-type current (I_M) in HVC_{RA}. A summary of the characterizing properties and dynamics of I_D and I_M is presented in the following section.

2.7 Review: D-current and M-current

2.7.1 The delay current I_D

The D current was first detected in hippocampal CA1 pyramidal neurons (Storm 1988, 1990). I_D has slow kinetics, particularly inactivation and recovery from inactivation. I_D activates at a low threshold; it is activated rapidly by depolarizations beyond -70 mV. It inactivates completely over several seconds and the recovery from inactivation is extremely slow (Storm 1990).

The classical role of I_D is to cause long delays (several seconds) to the first spike in response to long depolarizing stimuli (Storm 1988, 1990). This is due to the rapid activation of I_D upon depolarization, keeping the cell from depolarizing any further. As I_D slowly inactivates, the cell slowly depolarizes in a ramp-like way until it reaches the spiking threshold and fires with a delay. Additionally, I_D was shown to reduce the firing frequency,

control action potential threshold (Shu et al. 2007), and contribute to irregular spiking discharge (Porter et al. 1998; Toledo-Rodriguez et al. 2004). I_D is sensitive to mM concentrations of DTX and μM concentrations of 4-aminopyridine (4-AP). The functions of I_D in various types of central neurons are summarized in **Table 1**.

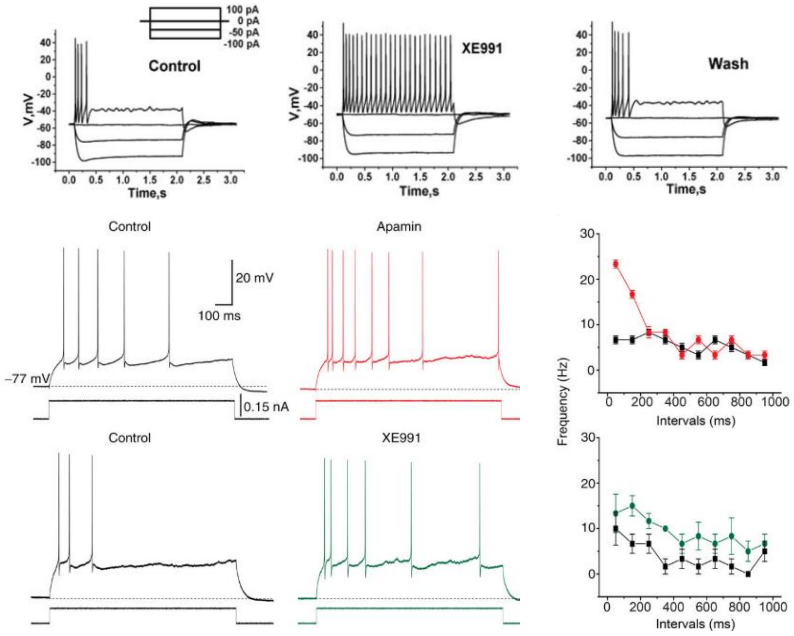

Figure 15 Rat sympathetic neurons fire one or few spikes in response to current pulses. Bath application of XE991 in rat converted firing from phasic to tonic (Zaika et al. 2006). (b) Rat dentate granule cells express M and SK channels. Bath application of Apamin (SK channel blocker) (red trace, top middle) or XE991(M-channel blocker) (green trace, bottom middle) increased excitability. Averaged firing frequencies measured within 100 ms time windows during 1 s, 0.15 nA current pulses. Apamin (top panel to the right) significantly increased the firing frequency during the first 200 ms of the pulse. However, XE991 (bottom panel to the right) increased the frequency during the whole 1 s response (Mateos-Aparicio et al. 2014)

I_D is similar to the A-type potassium current (I_A) (Storm 1988, 1990); both currents are sensitive to 4-AP and delay the firing discharge. However, I_A is very much less sensitive to 4-AP, requiring 1-5 mM for a block, while micromolar concentration of 4-AP (~40 µM) is sufficient to block I_D. I_A can cause delays up to 100 ms while I_D causes far longer delays (several seconds). Furthermore, I_D has slower kinetics than I_A, I_D inactivates and recovers from inactivation more slowly. I_D has also more negative thresholds for activation and inactivation than I_A.

Additionally, I_D resembles the low threshold, slowly inactivating potassium current found in neurons of the ventral cochlear nucleus (I_{LT}) (Rothman and Manis 2003). Similarly, I_{LT} is sensitive to DTX and inhibits repetitive firing. However, I_{LT} incompletely inactivates and has not been shown to cause delayed discharge.

2.7.2 M-type current (I_M)

The M-current was originally described by Brown and Adams (1980) in frog sympathetic neurons (Brown and Adams 1980) as a non-inactivating K^+ current that was inhibited by muscarinic acetylcholine receptor stimulation, thus its name M-current. I_M is voltage-dependent; it activates slowly by depolarization at subthreshold potentials, from about -60 mV. It does not inactivate; this assists in stabilizing the membrane potential in presence of depolarizing currents. Because of its slow activation, it does not contribute to individual spike repolarization.

I_M mainly serves as a brake for repetitive firing; once activated (slowly) by depolarization, it generates an enhanced outward current following the initial spike burst, therefore, raising the threshold for subsequent spikes. The inhibition of M-current by either XE991 or linopirdine, hence, leads to enhanced neuronal excitability. Additional functions for I_M have been demonstrated. I_M contributes to SFA in sympathetic (Brown and Passmore 2009)and hippocampal (Simon P Aiken et al. 1995; Brown and Passmore 2009) neurons. It controls AP threshold and suppresses spontaneous firing (Shah et al. 2008): blocking I_M in hippocampal neurons reduces the action potential threshold by around 7-8 mV resulting in spontaneous firing of many neurons. These functions are summarized in **Table 2**

Table 1 : Functions of the delay current I_D mediated by Kv1 channels in mammalian central neurons

LOCATION/NEURON	CHANNEL SUBUNIT	PHARMACOLOGICAL BLOCKER	FUNCTION	REFERENCE
Axonal cortical neurons	Kv1.2	TsTx	Affects axonal spike threshold Suppresses firing Slow ramp upon prolonged depolarization Spike repolarization	(Shu et al. 2007) PNAS
Rat Neocortex	Kv1.1	DTX-I(1.1, 1.2, 1.6) DTX-K (kv1.1)	Correlated with STUT discharge	(Toledo-Rodriguez et al. 2004) Cerebral Cortex
Gabaergic interneurons in the rat neocortex	Kv1.1 (at least)	DTX-I, DTX-K	Responsible for irregular discharge	(Porter et al. 1998) European Journal of Neuroscience

Pyramidal Neurons of the Layer II and layer III of rodent granular retrosplenial cortex	Kv1.1 (at least)	DTX-I, DTX-K	late spiking	(Kurotani et al. 2013) Brain Structure and Function
Motor spinal neurons of rodents	Kv1.2	TsTx	delayed spike discharge with a slow ramp setting the RMP promote a slow acceleration in firing rate because of its slow inactivation	(Bos et al. 2018) Cell Reports
Striatal medium spiny neurons of the rat striata	Kv1.2	DTX-I(1.1, 1.2, 1.6)	Delay to 1st spike Reduction of firing frequency	(Shen et al. 2004) Journal of Neurophysiology

Table 2 Functions of Kv7 channels in mammalian central neurons

LOCATION/NEURON	CHANNEL SUBUNIT	PHARMACOLOGICAL BLOCKER	FUNCTION	REFERENCE
Rat sympathetic Neuron	Kv7	Linopirdine	Inhibition of repetitive firing Contribute to SFA	(Zaika et al. 2006) J. Physiol (Brown and Passmore 2009) British Journal of Pharmacology
Rat hippocampal CA1 pyramidal neurons	Kv7	Linopirdine	Suppress endogenous burst firing followed by an afterdepolarization Control of AP threshold Stabilize the RMP Contribute to SFA Inhibit firing	(Simon P. Aiken, Lampe, and Brown 1995) British Journal of Pharmacology (Brown and Passmore 2009) British Journal of Pharmacology
Rat hippocampal dentate granule cells	Kv7	XE991	control AP threshold → Blocking M-current shifts Vth to more negative values Dampening of excitability	(Mateos-Aparicio et al. 2014) J Physiol.

2.8 Previous models of HVC_{RA}

Computational models of neuronal circuits serve as a framework for generating hypotheses about cell type specific role in an active network. The behavior of the circuit depends on the intrinsic properties of component neurons and the dynamics of their interaction. Numerous models have been proposed to investigate the HVC circuitry and how neurons within are interconnected (Gibb, Gentner, and Abarbanel 2009; Jin, Ramazanoğlu, and Seung 2007; Long et al. 2010). These models were either biophysically nonrealistic incorporating non-ionic forms of conductance-based models or failed to replicate the behavior of neuronal discharge. Moreover, the diversity of cellular properties of HVC cell types are rarely incorporated because the full complement of channels expressed by HVC neurons was not known. Arij Daou and his co-workers in 2013 completed the latest model of HVC in an attempt to replicate the firing patterns of HVC_X, HVC_{RA}, and HVCint. While the spiking patterns of HVC_X and HVCint were successfully reproduced, however, the model failed to replicate HVC_{RA}'s firing activity. HVC_{RA}'s model failure was due to an inaccuracy in the ionic currents composing that model. For instance, they attributed the delay in firing to the expression of the A-type current (I_A) solely. They confirmed the presence of I_A in that study by applying a 0.3 mM dose of 4-AP. However, 4-AP is a non-selective blocker that inhibits I_A and I_D. I_A is sensitive to mM concentrations of 4-AP while I_D is sensitive to micromolar concentrations of 4-AP. Thus, the 0.3 mM dose of 4-AP used in that study may have blocked I_A and/or I_D. Therefore, the delay may be dependent on the presence of either or both currents. Furthermore, the model trace poorly matched HVC_{RA}'s experimental trace and the stuttering pattern of HVC_{RA} wasn't replicated as well.

CHAPTER 3

METHODOLOGY

This chapter summarizes the computational approach adopted to simulate the electrical activity of HVC_{RA} neurons. An overview of the model fitting procedure will be presented first, followed by a description of the developed model and then the framework adopted to assess the goodness of the fitted model traces.

3.1 Model fitting procedure

Figure 16 depicts the basic workflow for model production and validation. In short, we constructed a single-compartment conductance-based model that generates predictions of the mixture of ionic currents controlling the electrical activity of HVC_{RA}. Densities of somatic conductances and additional parameters are manually adjusted to match the voltage model trajectory to the biological trace in response to step current. The goodness of the fitted trace is assessed by comparing intrinsic features of interest (e.g., spike rate, spike width) of the experimental voltage trajectory and model response. For each electrophysiological feature, the error is calculated as an absolute z-score (Druckmann et al. 2007). Errors are then averaged together to produce a single objective error function (Gouwens et al. 2018). Next, we will evaluate how the model trace performed on additional stimuli upon which it was not fitted. Similarly, the predicted trace is evaluated by calculating the error of intrinsic features of interest and averaging them together. Finally, predictions about the ionic currents

present will be tested and verified in the slice using pharmacological manipulations (DTX to test the existence of the D-current (Shu et al. 2007), XE991 to test the presence of the M-current (Brown and Passmore 2009)).

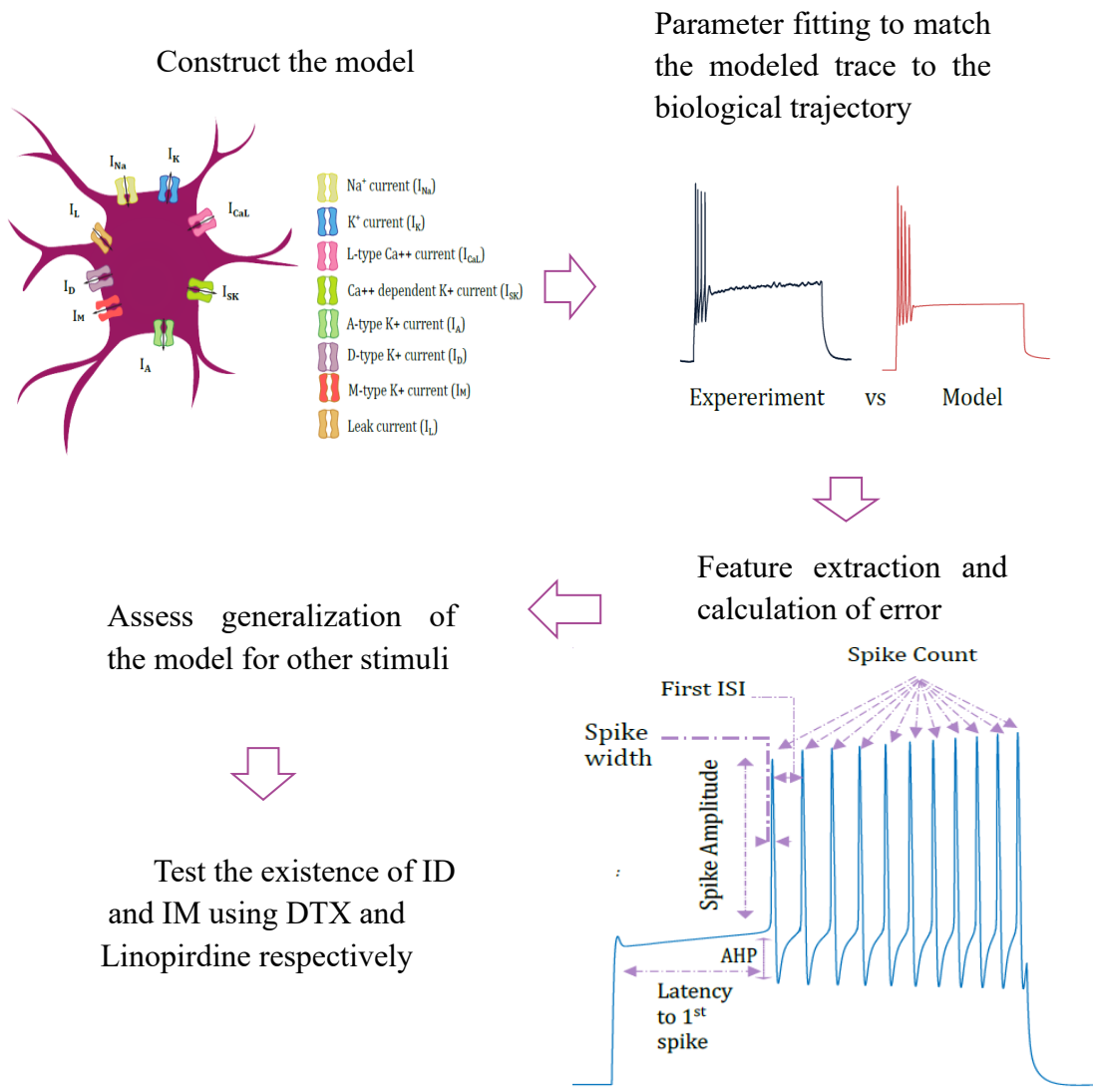

Figure 16 Schematic showing the basic workflow for model production and validation.

3.2 HVC$_{RA}$ model

We constructed a Hodgkin and Huxley like single-compartment conductance-based model comprised of spike producing currents (I_K and I_{NA}), a small conductance calcium-activated potassium current (I_{SK}), a high threshold L type calcium current (I_{CaL}), a slowly inactivating D-type potassium current (I_D), a non-inactivating M-type potassium current (I_M), an A-type potassium current (I_A), a leak current (I_L). and an external applied current (I_{app}) to drive spiking. I_{SK} is activated by intracellular calcium which enters the cell through high threshold L-type calcium channels. known to inhibit repetitive firing by hyperpolarizing the membrane potential following each action potential, thus, leading to an increase in interspike interval and decrease in spiking frequency (Faber 2009). It also contributes to SFA. I_D causes long delay to the first spike, slow membrane depolarization (ramp), irregular spiking or stuttering, and suppresses repetitive firing. I_M, similarly, inhibits firing and contributes to SFA. I_A generates delay in spiking (~0.1s) and reduces the firing frequency.

The membrane potential V is described by the following first-order differential equation:

$$Cm\frac{dV}{dt} = I_{app} - (I_{Na} - I_K - I_{CaL} - I_{SK} - I_D - I_M - I_A - I_L)$$

where Cm is the membrane conductance.

I_K, I_K, I_{CaL}, I_D, I_M, and I_A are voltage-dependent currents, while I_{SK} depends on the concentration of intracellular calcium. The voltage-dependent currents are modeled using Hodgkin-Huxley formalism, so that for each current:

$$I = gm^x h^y (V - E)$$

Where g is the maximal conductance, x and y are the numbers of gate activation and inactivation variables, respectively; E is the reversal potential of the ion involved, and V is the membrane potential.

In these equations, currents are governed by an activation/inactivation variable x whose rate of change is defined by the following first-order differential equation

$$\frac{dx}{dt} = \frac{x_\infty - x}{\tau_x}, \qquad x = \text{h, n, e, w, z or y}$$

where τ_x is the time constant of x, x_∞ is the steady-state value of x, and x itself represents the activation/inactivation variables h, n, e, w, z, y, and r in the following equations, whereas θ_x, $x = m, n, s, w, z, y, a \; or \; e$ is the half-activation/inactivation voltage for gating variable x and σ_x, $x = m, n, s, w, z, y, a \; or \; e$ is the slope factor for that variable.

3.2.1 Defining the currents

The voltage-dependent model currents

Spike producing currents Na^+ and K^+ (Daou et al. 2013)

$$I_{Na} = g_{Na} m_\infty^3(V) h (V - V_{Na})$$

$$m_\infty = \frac{1}{1 + \exp\left(\frac{V - \theta_m}{\sigma_m}\right)}$$

$$\alpha_h = 0.128\exp\left(\frac{V+50}{18}\right)$$

$$\beta_h = \frac{4}{1+exp\left(\frac{-(V+27)}{5}\right)}$$

$$h_\infty = \frac{\alpha_h}{\alpha_h+\beta_h}$$

$$I_K = g_K n^4 (V - V_K)$$

$$n_\infty = \frac{1}{1+\exp\left(\frac{V-\theta_n}{\sigma_n}\right)}$$

$$\tau_n = \frac{10}{\cosh\left(\frac{V-\theta_n}{2\sigma_n}\right)}$$

L-Type Ca^{2+} current (Daou et al. 2013)

$$I_{CaL} = g_{Ca} V s_\infty^2(V)\left(\frac{Ca_{ex}}{(1-exp\left(\frac{2FV}{RT}\right)}\right)$$

$$s_\infty = \frac{1}{1+exp\left(\frac{V-\theta_s}{\sigma_s}\right)}$$

The term $\frac{F}{RT}$ is the thermal voltage, where T is the temperature of the bathing solution (25°C or 298 K), R is the gas constant, and F is Faraday's constant. Ca_{ex} is the external Ca^{2+} concentration, which is 2.5 mM in the bathing solution.

The low threshold slowly inactivating delay current I_D (Shu et al. 2007)

$$I_D = g_D wz(V - V_K)$$

$$w_\infty = 1 - \frac{1}{1 + exp\,(\frac{V - \theta_w}{\sigma_w})}$$

$$z_\infty = \frac{1}{1 + exp\,(\frac{V - \theta_z}{\sigma_z})}$$

The low threshold non inactivating M-type current (I_M) (Ross et al. 2017)

$$I_M = g_M y(V - V_K)$$

$$y_\infty = \frac{1}{1 + exp\,(\frac{-(V - \theta_y)}{\sigma_y})}$$

The A-type current I_A (Daou et al. 2013)

$$I_A = g_A a_\infty(V) e(V - V_k)$$

$$a_\infty = \frac{1}{1 + exp\,(\frac{V - \theta_a}{\sigma_a})}$$

$$e_\infty = \frac{1}{1 + exp\,(\frac{V - \theta_e}{\sigma_e})}$$

The voltage-independent currents

Ca^{2+} dependent potassium current I_{SK}

$$I_{SK} = g_{SK} k_\infty([Ca^{2+}]_i)(V - V_k)$$

Where $k_\infty([Ca^{2+}]_i)$ is the steady-state activation function of the SK current that is based on the levels of intracellular calcium and is given by:

$$k_\infty([Ca^{2+}]_i) = \frac{[Ca^{2+}]_i^2}{[Ca^{2+}]_i^2 + k_s^2}$$

The constant k_s is the dissociation constant of the Ca^{2+}-dependent current, and $[Ca^{2+}]_i$ is the intracellular concentration of free Ca^{2+} ions and is governed by

$$\frac{d[Ca^{2+}]_i}{dt} = -f\{\varepsilon I_{Ca} + k_{Ca}([Ca^{2+}]_i - b_{Ca})\}$$

The constant f represents the fraction of free-to-total cytosolic Ca^{2+}. The constant ε combines the effects of buffers, cell volume, and the molar charge of calcium. Also, the constant k_{Ca} is the calcium pump rate constant, and b_{Ca} represents the basal level of Ca^{2+}.

The leak current IL

$$I_L = g_L(V - V_K)$$

Simulations consisted of solving for the membrane voltage (V) in response to the injected current $Iapp$. To match the model voltage trace to the biological trajectory, we manually fitted several parameters in the model that directly influences the action potential shape (amplitude, width, afterhyperpolarization (AHP), spike train, and particular features of interest (latency/delay to spike, stuttering, SFA...) of the output trajectory. Thus, maximal conductances of the different ionic currents along with the membrane capacitance Cm were adjusted to control firing frequency and match gross features of individual spikes (spike amplitude, AHP). For more subtle control over the spike shape, half activation of Na^+ and K^+ currents were fitted. Furthermore, activation and/or inactivation time constants, in addition to activation and or inactivation level of the delay current I_D and M-type current I_M were calibrated to capture subtle aspects of firing (latency, spike timing...). Parameter values that remained constant across all simulations are presented in Table 3. Model resolution and parameter fitting were implemented in MATLAB using a built-in graphical user interface.

3.3 Model assessment

To judge the goodness of fit, we extracted a set of features from the fitted and biological responses to positive current injections. The physiological features measured are illustrated in **Figure 17**. Across all modeled and biological traces, 1st spike amplitude, width, and afterhyperpolarization (AHP), along with the first and second interspike interval (ISI) were computed. The first spike amplitude was computed as the difference between peak spike value and minimum value of spike afterhyperpolarization. Spike width is measured at half maximal amplitude, AHP is measured as the difference between spike threshold and

minimal value of spike afterhyperpolarization, and ISI is calculated as the difference of peak timing of two consecutive spikes

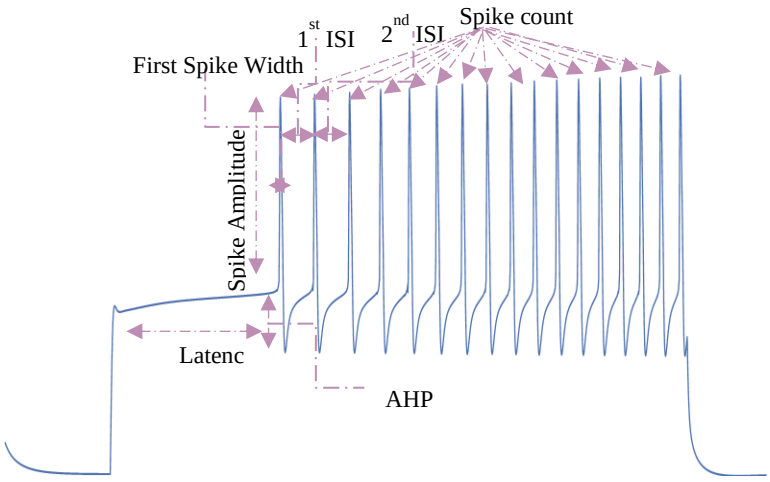

Figure 17 Feature extraction to assess the goodness of fit. The first spike amplitude is calculated as the difference between peak spike value and minimum value of spike afterhyperpolarization. Spike width is measured at half maximal amplitude, AHP is measured as the difference between spike threshold and minimal value of spike afterhyperpolarization, and ISI is measured as the difference of peak timing of two consecutive spikes)

Table 3: Constant parameter values

Parameter	Value	Parameter	Value	Parameter	Value
$\boldsymbol{\theta_s}$	-20 mV	τ_h	1 ms	b_{Ca}	0.1 μM

$\boldsymbol{\theta_y}$	-45 mV	τ_e	20 ms	ε	0.0015 $\mu M/(pA.ms)$
$\boldsymbol{\theta_a}$	-20 mV	V_K	-90 mV		
$\boldsymbol{\theta_e}$	-60 mV	V_{Na}	50 mV		
$\boldsymbol{\sigma_s}$	-0.05 mV	V_L	-70 mV		
$\boldsymbol{\sigma_y}$	5 mV	k_{Ca}	0.3 ms-1		
$\boldsymbol{\sigma_a}$	-10 mV	f	0.1		
$\boldsymbol{\sigma_e}$	5 mV	k_s	0.5 μM		

CHAPTER 4

RESULTS

Results are presented in two sections. First, we describe the ability of the delay current I_D, M-type current I_M to represent the characterizing features of HVC_{RA} to step evoked firing response observed *in vitro*. In the following section, the fitted model traces to the real response of HVC_{RA}, are shown. Model confirmation by the pharmacological manipulations is then presented next. Finally, results of the model assessment are shown.

4.1 Influence of I_D and I_M on spiking patterns

4.1.1 Influence of I_D on firing patterns

To determine to which extent the D-current can account for the phasic, stuttering, and delayed firing patterns observed in HVC_{RA} responses *in vitro*, we constructed a model consisting of I_{Na}, I_K, and I_D. Interestingly, we found that these patterns mainly depend on the availability of I_D (g_D) and its inactivation time constant (τ_z). The inactivation time constant τ refers to how long the ion channel takes to close. The higher the value of τ the longer the time the channel takes to inactivate.

Sixteen simulations in response to 350 pA current pulse, with varying g_D and τ_z. are shown in **Figure 18**. As g_D is increased, firing response transitions from long trains of action potentials to discontinuous spiking or STUT followed by delayed or phasic firing. For low values of τ_z , the model fires in a delayed pattern, while at higher values, the model fires a

single spike. Thus, as I_D inactivates more slowly, and at high magnitudes of g_D, the model tends to fire in a phasic pattern.

Examining the resulting voltage traces, a slow membrane potential depolarization is elicited (i) during the long delay to spike, (ii) following the single spike during phasic firing, and (iii) between separate bursts of action potentials during stuttering (STUT). The transitioning from a sustained to either a phasic, STUT or delayed response was relatively rapid and characterized by a differential drop in firing frequency depending on τ_z. The longer the channel takes time to inactivate, the faster the drop in firing frequency. Furthermore, a certain level of $g_D$is necessary to convert spiking; the simple presence of I_D is not enough to create a phasic, delayed, or stuttering response. Once g_D reaches a critical value, the rapid activation of I_D generates an enhanced outward current, converting the firing pattern. As I_D inactivates slowly, the cell membrane depolarizes in a ramp-like way. It is only when the cell reaches the threshold of spiking it fires a delayed or second burst of spikes. Thus, I_D is accountable for generating the phasic, delayed, and STUT patterns.

Furthermore, we sought to investigate the influence of I_D on the firing frequency for varying values of τ_z. Thus, we evaluated the model's firing frequency in response to increasing magnitudes of applied current, at different levels of τ_z. As illustrated in **Figure 19**, a progressive increase in firing frequency.is elicited at low values of τ_z, however a sudden jump in firing is generated at higher levels of τ_z, indicating the fast transition from a phasic to tonic spiking. Thus, the longer the channel takes time to inactivate, the faster the transition from a phasic activity at low applied current to a tonic firing at higher steps of stimulation current.

To examine the effect of I_D on the rheobase, we compared the change in firing frequency in response to increasing step currents when I_D is blocked (g_D= 0) (**Figure 20**). When I_D is present, firing shifted abruptly from phasic to tonic activity in response to increasing current pulses. The minimal current needed to elicit a spike (rheobase) was 100 pA. Blocking I_D (g_D =0) lowered the rheobase (5 pA vs 100 pA for control), increased the spiking activity over the entire range of current injections, and blocked the abrupt increase in spike count.

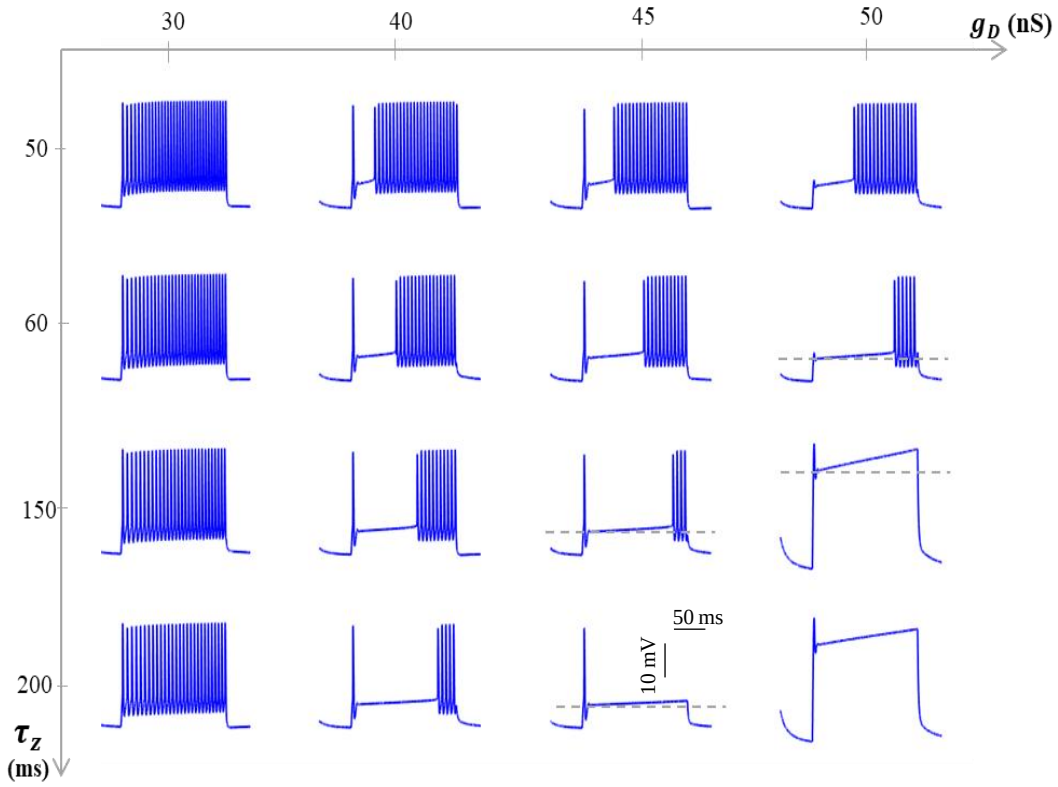

Figure 18 Influence of I_D on firing patterns. Phasic, STUT and delayed patterns depend on the availability of I_D (g_D) and its inactivation time constant (τ_z). Dashed gray lines delineate the ramp.

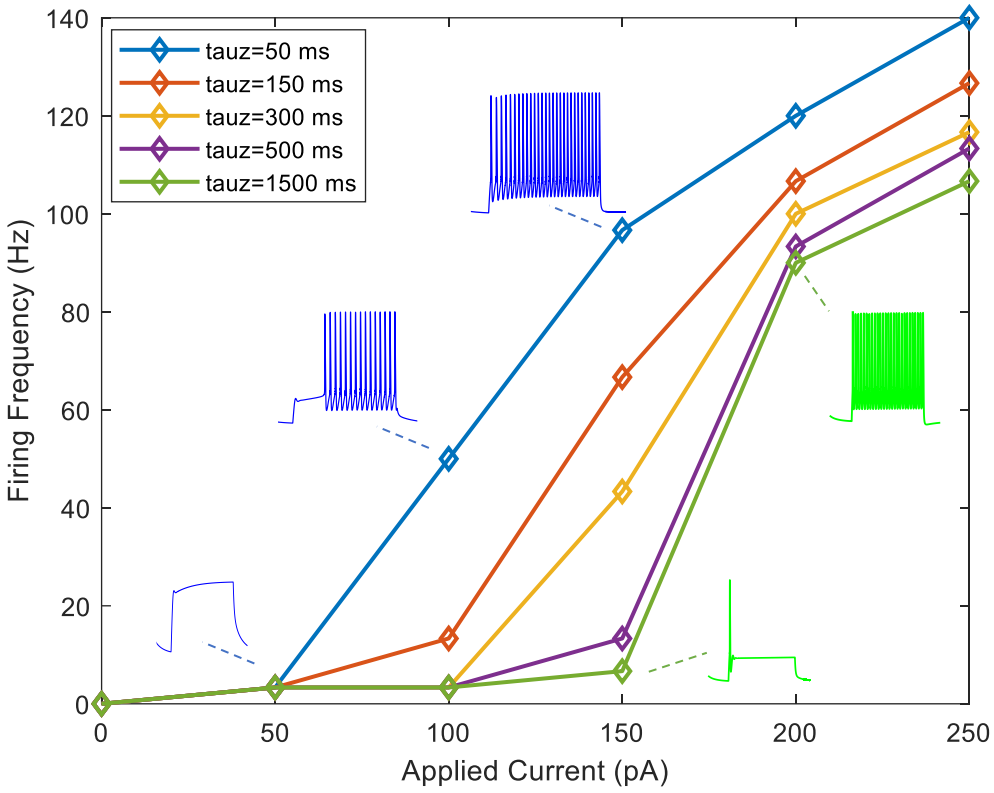

Figure 19 Influence of I_D on the firing frequency for varying values of τ_z. The longer the channel takes time to inactivate, the faster the transition from a phasic activity at low applied current to a tonic firing at higher steps of stimulation current

4.1.2 Influence of I_M

To examine the modulation of M-current on intrinsic excitability, we constructed a model consisting of I_{Na}, I_K and I_M. The resulting simulations in response to a 350 pA stimulation current are displayed in **Figure 21**. Increasing g_M progressively reduced the firing rate, preventing the cell from generating further action potentials. At intermediate magnitudes of g_M, firing was characterized by a late spike frequency adaptation (progressive increase in interspike interval). As g_M is further increased, firing was further suppressed

resulting in a phasic response. The initial spikes are followed by a stabilization of the membrane potential. The slow activation of I_M generates an outward current that raises the threshold for subsequent spikes, thus abbreviating spike discharge. The lack of inactivation of I_M assists in stabilizing the membrane potential in presence of a depolarizing stimulus.

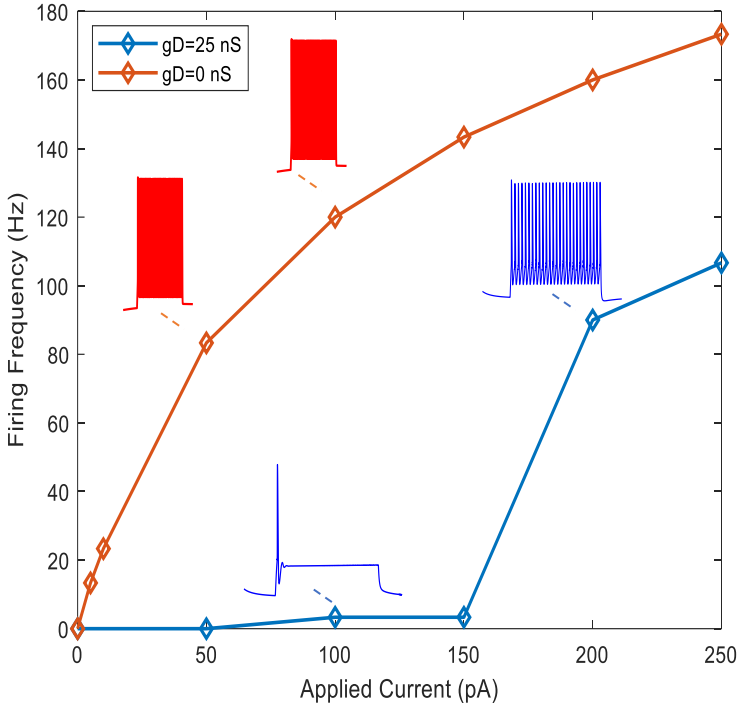

Figure 20 Effect of I_D on the rheobase. Blocking I_D (g_D =0) lowered the rheobase (5 pA vs 100 pA for control), increased the spiking activity over the entire range of current injections, and blocked the abrupt increase in spike count. Blue and red traces correspond to the voltage responses.

Furthermore, we studied the model response to increasing step currents (**Figure 22**). The model fired phasically in response to the rheobase (50 pA). As the stimulation current

is incremented, the firing rate increased progressively, shifting from a single spike to a few spikes. Blocking I_M (g_M =0) greatly increased the firing rate and shifted the rheobase to lower values (50 pA vs 5 pA for control)

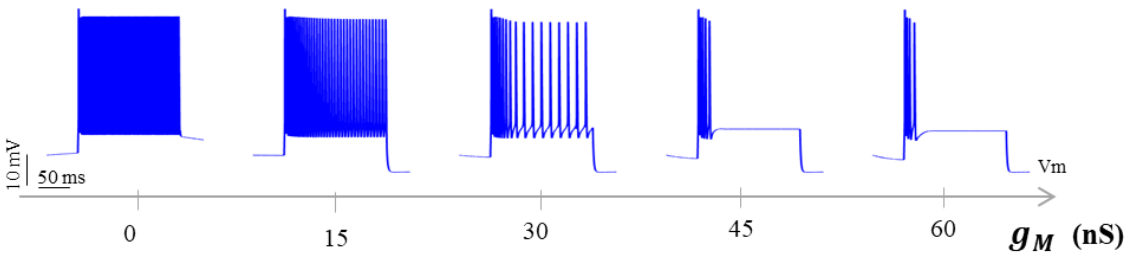

Figure 21 Influence of I_M on firing. Increasing g_M progressively reduced the firing rate, preventing the cell from generating further action potentials

4.1.3 Influence of I_M and I_D

To examine the effect of both currents I_M and I_D on firing, we constructed a model consisting of I_{Na}, I_K, I_M.and I_D. Interestingly, when both currents were present, the model resulted in a stuttering pattern similar to the actual electrical response of HVC_{RA}. **Figure 23** summarizes the ionic mechanism underlying this discontinuous spiking. First, the rapid activation of I_D at low threshold upon depolarization suppresses firing. As I_D slowly inactivates, the cell slowly depolarizes in a ramp-like way until it reaches the spiking threshold and fires a second burst of action potentials. However, the slow activation of I_M and its lack of inactivation generates an enhanced non-inactivating outward current following the second burst of spikes, causing late spike adaptation and further suppressing spike discharge.

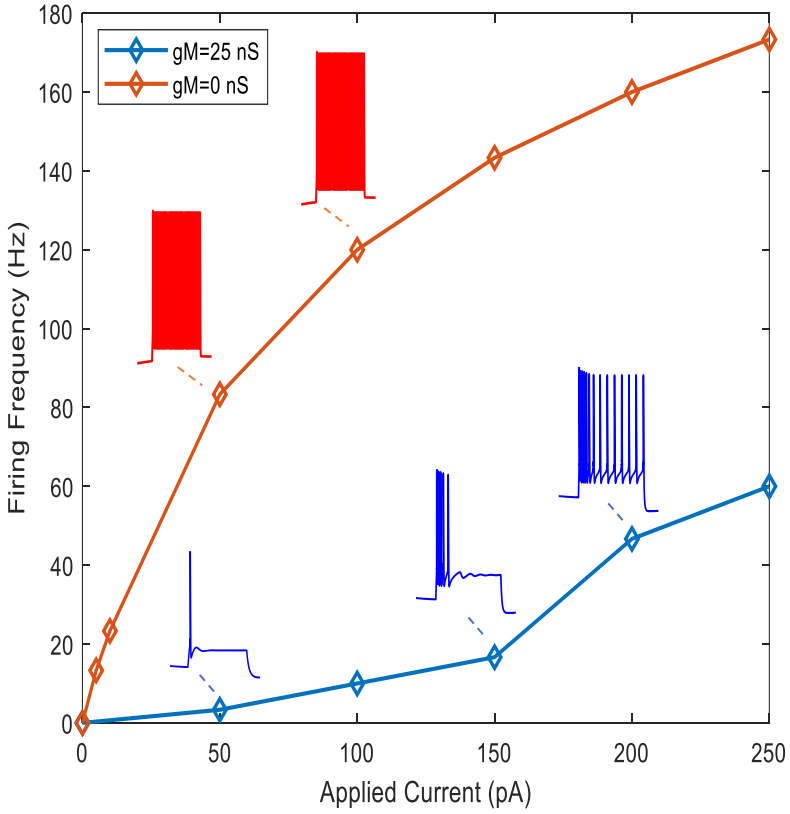

Figure 22 Effect of I_M on the rheobase Blocking I_M (g_M =0) greatly increased the firing rate and shifted the rheobase to lower values (50 pA vs 5 pA for control).

4.2 Model Results

4.2.1 Fitted traces

We have fitted the responses of 28 HVCRA neurons of 7 birds in total. Model parameters were calibrated to match the model output to the actual neuron's behavior in response to a depolarizing current injection. Model fits were tested by assessing model predictions in response to current injections not used in the fitting process. Good fits and

predictions of four neurons firing in different spiking phenotypes are shown in Figures 24-26. The model successfully replicated the diverse firing patterns in response to the current injections used in slice during current-clamp recording. As illustrated in Figures 24-26, the model captured the phasic, tonic, delayed, and STUT patterns characterizing HVC_{RA} activity.

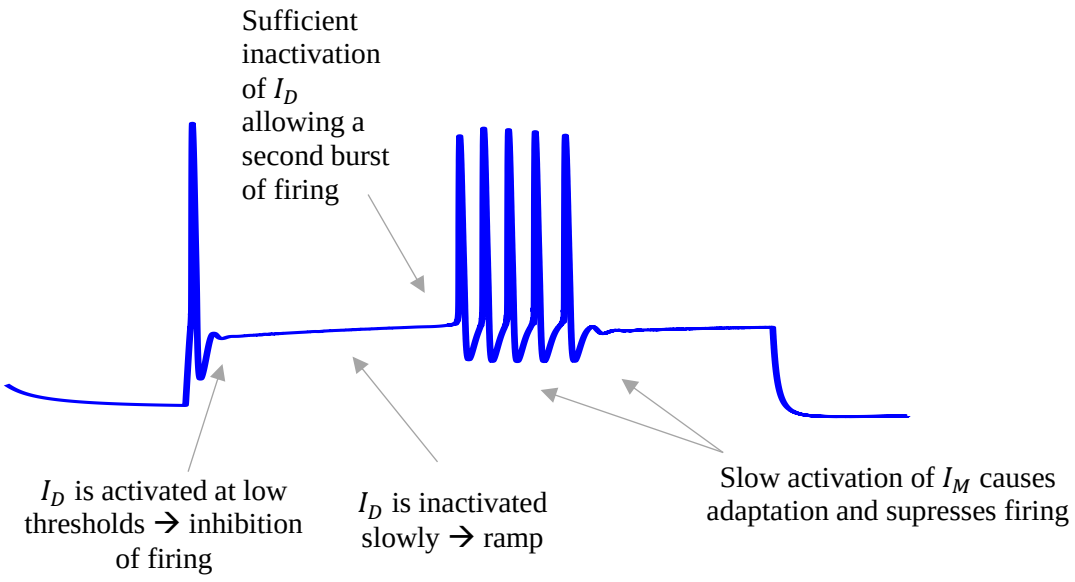

Figure 23 Summary of the roles of I_M.and I_D.in shaping the STUT pattern

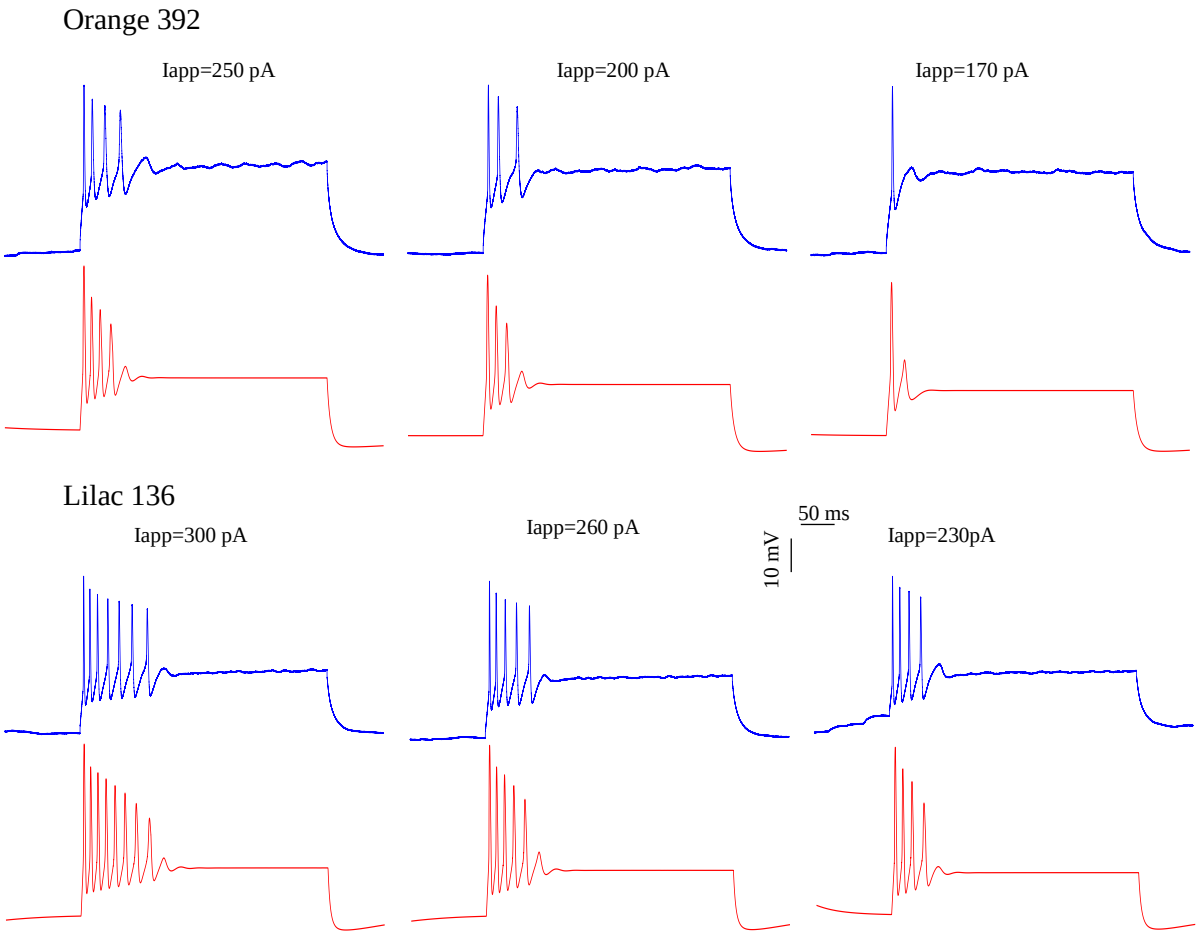

Figure 24 : Modeled (red traces) and experimental (blue traces) of 2 neurons (1 neuron/bird) firing phasically are displayed. Left are the fitted traces, middle and right are the predicted model responses

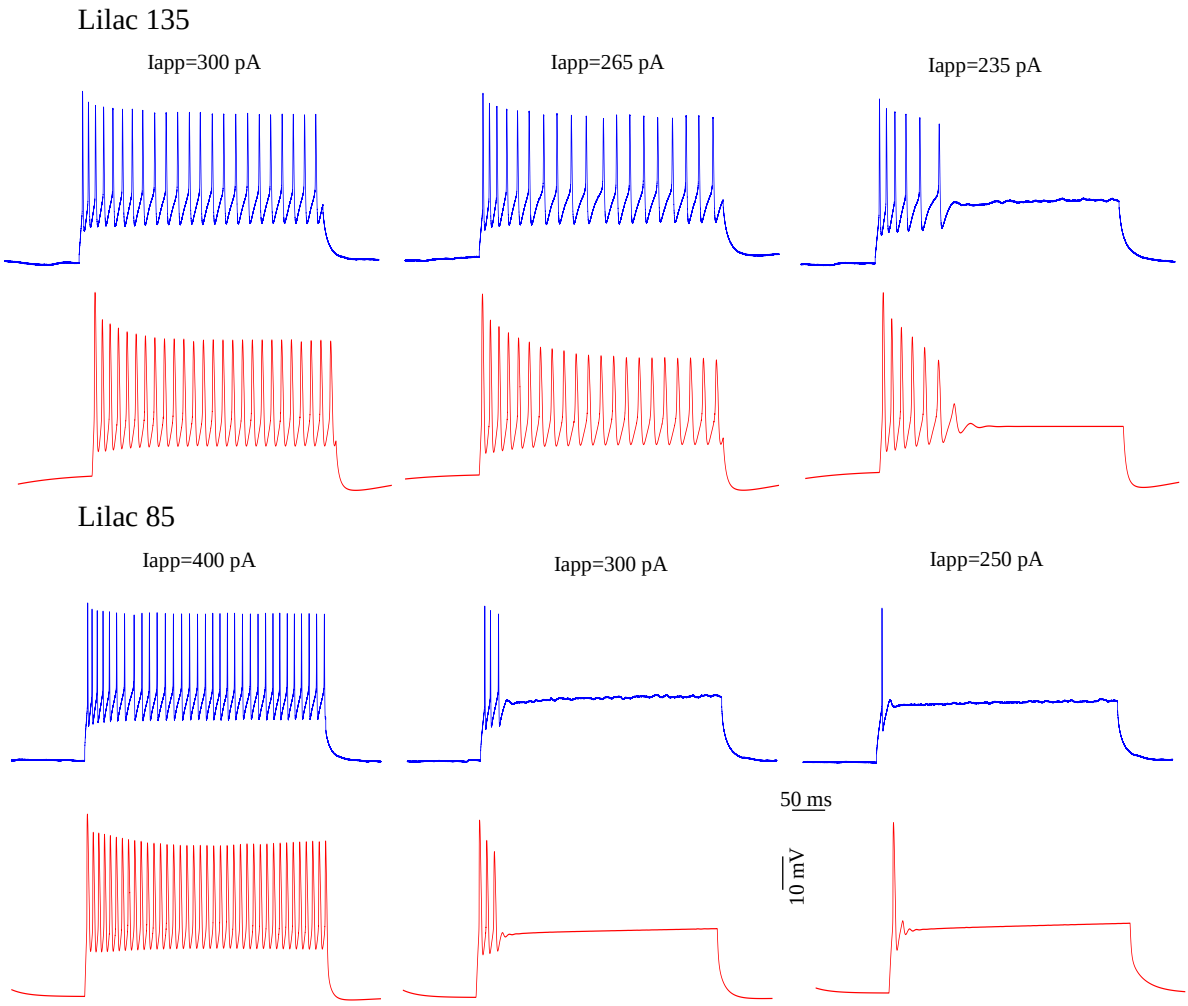

Figure 25 Modeled (red traces) and experimental (blue traces) of 2 neurons (1 neuron/bird) exhibiting tonic and phasic firing are displayed. Left are the fitted traces, middle and right are the predicted model responses.

4.2.2 Conductance space

Maximal ionic conductances of I_{Na}, I_K, I_A, I_{CaL}, I_{SK}, I_M, and I_D along with additional parameters were calibrated to match the neuron's actual response. Fitting mainly depended on calibrating the maximal conductances of I_M, I_D, and I_{SK} and activation and inactivation

time constants of I_M and I_D respectively to reproduce the firing patterns observed in vitro. Examining the distribution of the predicted current magnitudes of I_M, I_D and I_{SK} revealed that neurons occupied three areas in the three-dimensional conductance space (**Figure 27**).

Results demonstrated that neurons' firing responses are either governed by the collective activity of I_D and I_{SK}, I_M and I_{SK} , or I_D I_{SK}, and I_M. Model responses governed by I_D and I_{SK} are characterized by (i) a phasic response followed by slow membrane depolarization in response to the rheobase, (ii) tonic firing with little to no adaptation in response to higher current steps, and (iii) a rapid increase in firing rate in response to increasing magnitudes of depolarizing current injections. In contrast, the model traces governed by I_M and I_{SK} are characterized by (i) a phasic response followed by membrane potential stabilization in response to the rheobase, (ii) a transient or sustained firing with spike frequency adaptation in response to higher current injections, and (iii) a progressive increase in firing rate under increasing magnitudes of depolarizing current injections. While neurons governed by the activity of the three potassium currents was are characterized by (i) a stuttering firing pattern and (ii) a slow and rapid increase of firing frequency in response to increasing magnitudes of step currents. Thus, neurons can be classified into three distinct types (types I, II, and III) based on the ion channels controlling their activity. Type I encompasses the cells in which I_D along with I_{SK} control the spike train, type II comprises the neurons where I_M and I_{SK} regulate the firing discharge, while type III encompasses neurons governed by the collective activity of these three potassium currents.

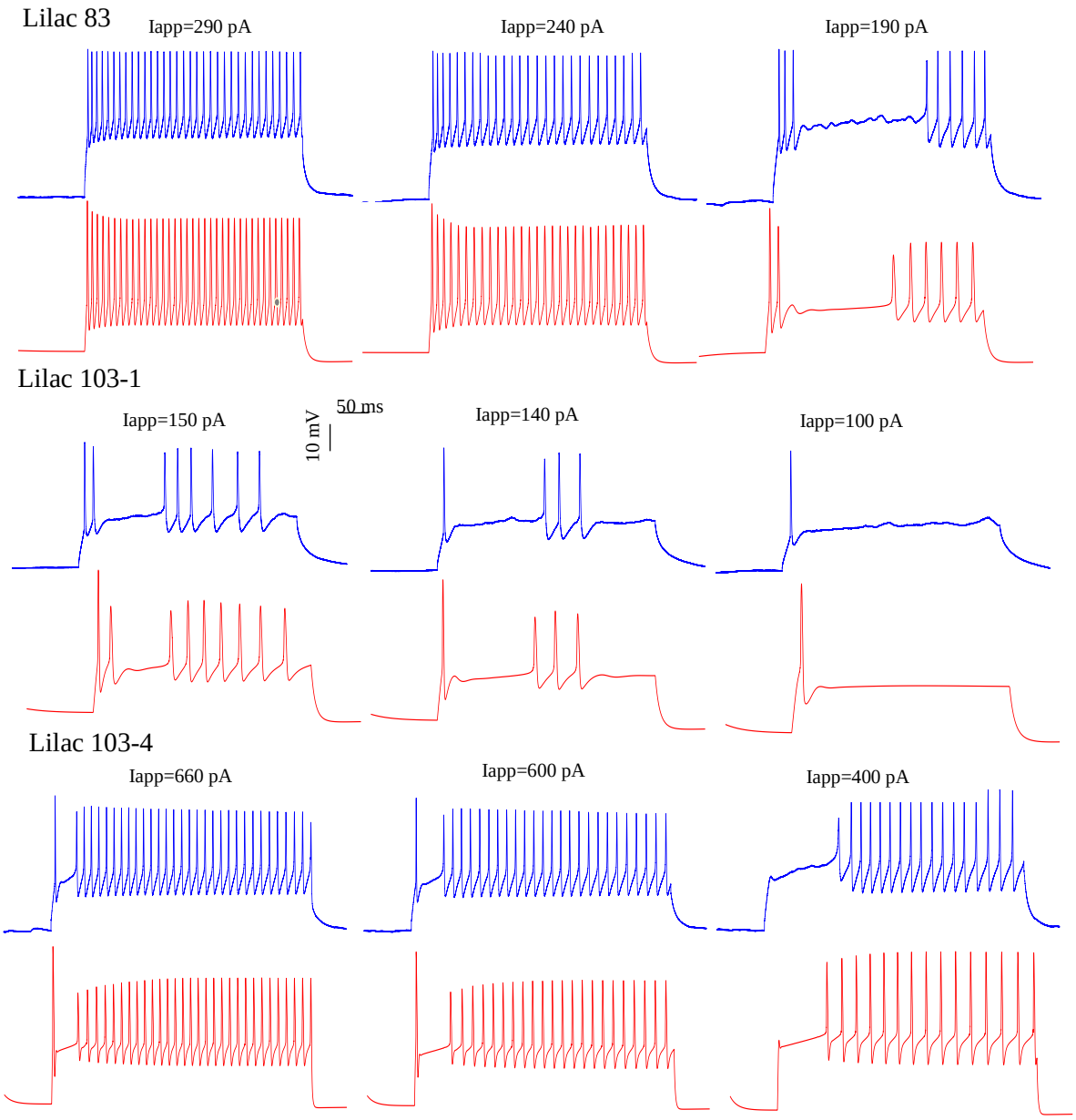

Figure 26 Modeled (red traces) and experimental (blue traces) of 3 neurons (1 neuron/bird) firing in STUT pattern are displayed. Left are the fitted traces, middle and right are the predicted model responses.

Mainly, M and D-currents govern the general spiking pattern of these three classes, however, I_{SK} contributes to the regulation of subtle features of firing and more specifically the interspike interval. I_{SK} is a calcium-activated potassium current that activates during an action potential, and the resultant hyperpolarization lowers the firing frequency and elongates interspike intervals.

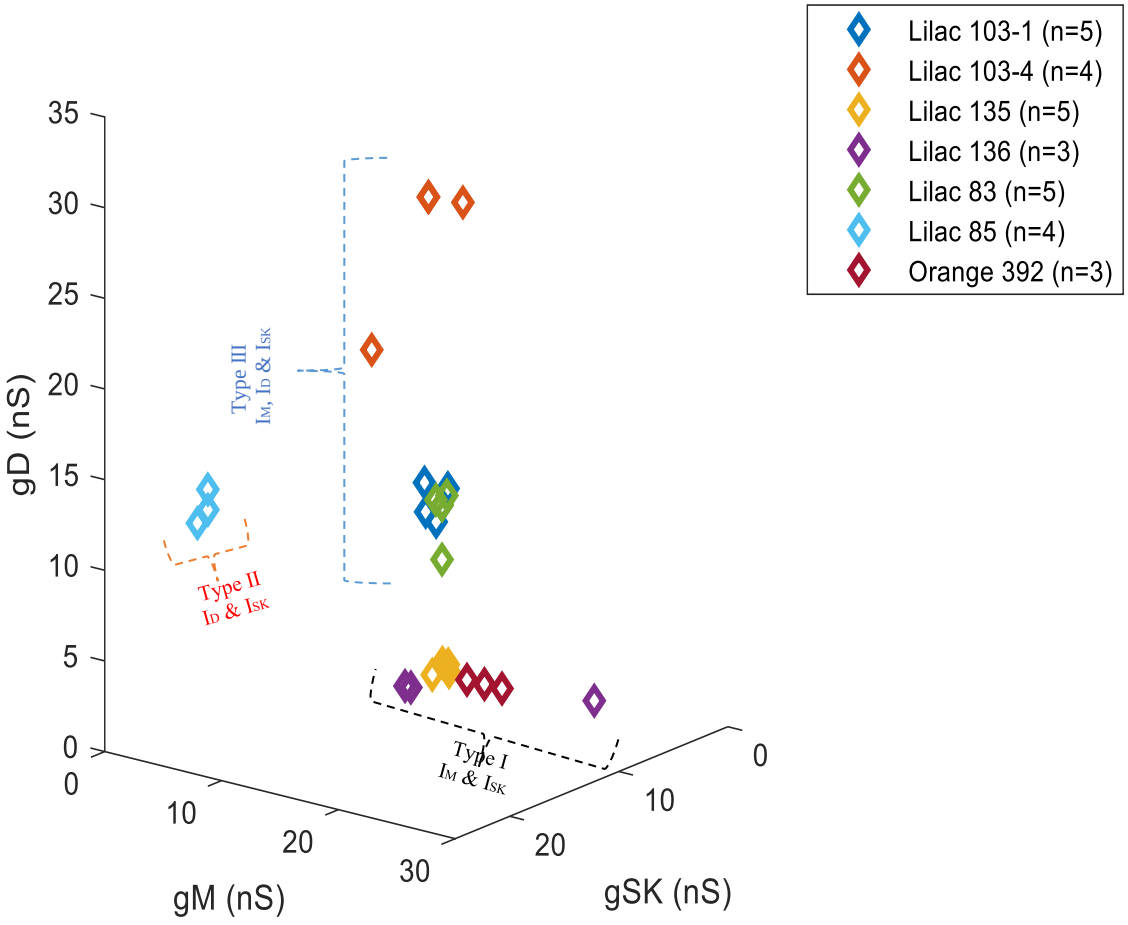

Figure 27 3D scatter plot of 28 modeled neurons showing the predicted conductances if I_{SK}, I_M and I_D. Each diamond refers to a neuron. Each bird is labeled by a color.

Figure 28 summarizes the different electrical activities classified within a single type. Neurons in Type I fire a single spike followed by stabilization of the membrane potential (due to the lack of inactivation of I_M) in response to the rheobase, while at higher applied currents it either fires a few spikes or tonically with adaptation. Neurons in type I are characterized by a progressive increase in firing frequency (**Figure 29**). Neurons in type II fire also phasically in response to the rheobase, however, the single spike is followed by a slow increase in membrane potential caused by the slow inactivation of I_D. At higher applied currents, neurons fire in a tonic with little to no adaptation resulting in a sudden increase in firing frequency. As for neurons in type III, they respond phasically or in a delayed pattern in response to the rheobase, while at higher applied currents, they fire in a discontinuous or stuttering pattern with adaptation. Neurons in this class either fire progressively or abruptly in response to increasing steps of applied current (**Figure 29**).

The model, in addition to replicating the diverse patterns, closely matched the firing rate *in vitro* for the three different classes.(**Figure 29**)

Classification of HVC_{RA} neurons into three types explained the diversity of firing based on gradients of potassium currents. However, within a single type, neurons tended to fire distinctively as well (**Figure 28**). The diversity within a single type is also explicated by the model. Simulations have shown that the ionic currents within a single type differ in their kinetic properties. For instance, neurons in type I either tend to fire tonically or phasically in response to high magnitude of applied current (**Figure 30**). By fitting these traces, we found that neurons firing tonically express an M-current with a faster activation time than neurons

firing phasically. In other words, the faster the M-current activates, the higher the frequency it fires at increased magnitudes of applied currents (**Figure 30**).

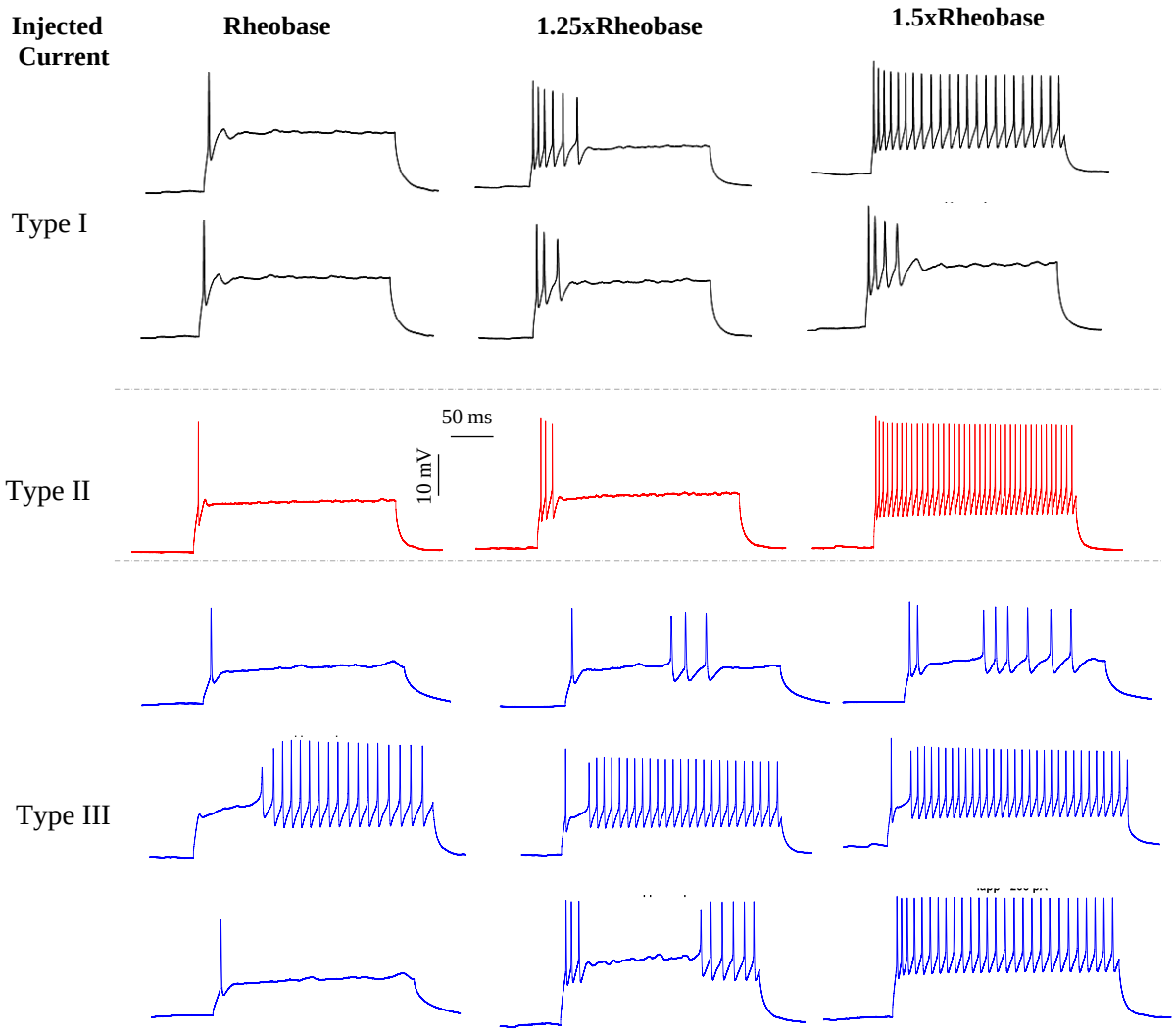

Figure 28 Classification of the diverse firing activities within three types. Each row corresponds to the response of a single neuron to the rheobase and higher amplitudes of applied current

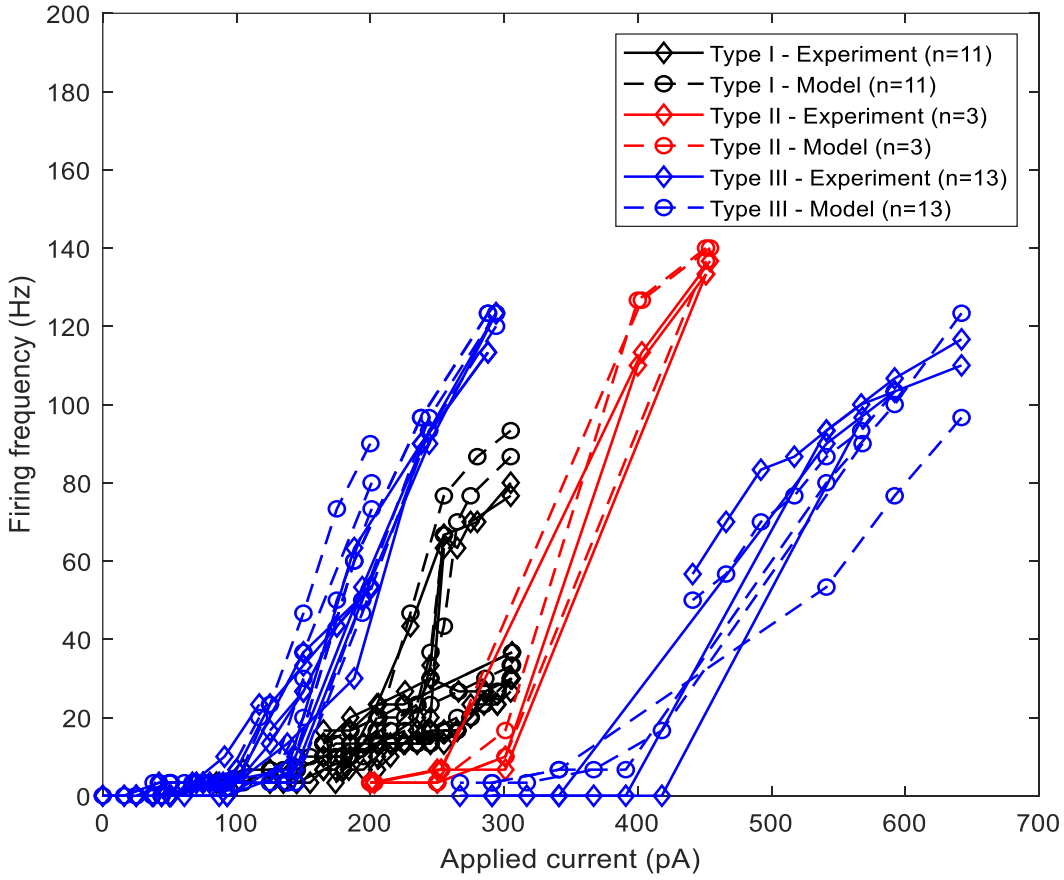

Figure 29 Firing frequency plotted against increasing current injections of 28 neurons of the model (circles) and experimental (diamonds) data are shown. Each color represents a cell type.

Additionally, variability arises within type III neurons (**Figure 28**) which is also explained by the model. Neurons within this class tend to fire irregularly (stuttering pattern) and distinctively. Fitting these diverse traces has shown that these neurons express a D-current that differentially inactivates across cells. We quantified these differences by

measuring the interspike interval separating two bursts of spikes (Max ISI) and plotted it against the inactivation time constant τ_z of I_D (**Figure 31**). We found that the Max ISI increases with higher values of τ_z. Meaning that the more time I_D takes to inactivate, the larger the distance separating two bursts of spikes.

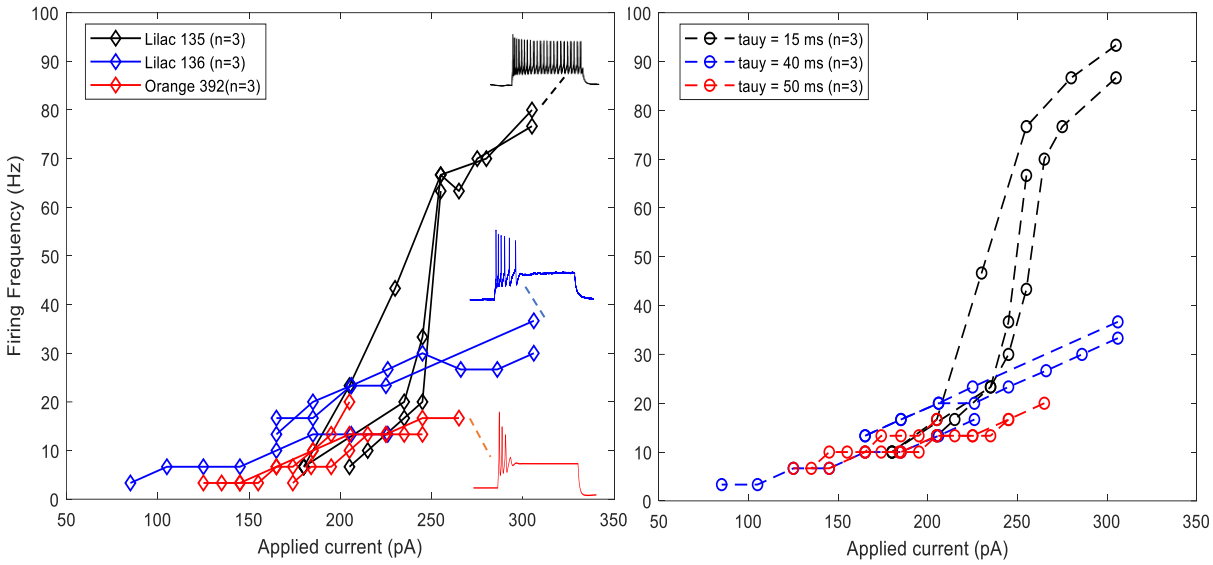

Figure 30 Variability within type I neurons. (Left) Neurons in type I either tend to fire tonically or phasically in response to high magnitude of applied current . . (Right) Simulated F-I curves of the neurons in the left panel. Each color corresponds to a bird. Neurons firing tonically express an M-current with faster activation time than neuron firing phasically.

To summarize, the diverse firing patterns exhibited in HVC_{RA} were classified into three distinct types based on gradients of low threshold potassium currents. Additionally, the distinct firing phenotypes within a single type were captured by the model and were shown

to be caused by differential activation and inactivation time constants of I_M and I_D respectively.

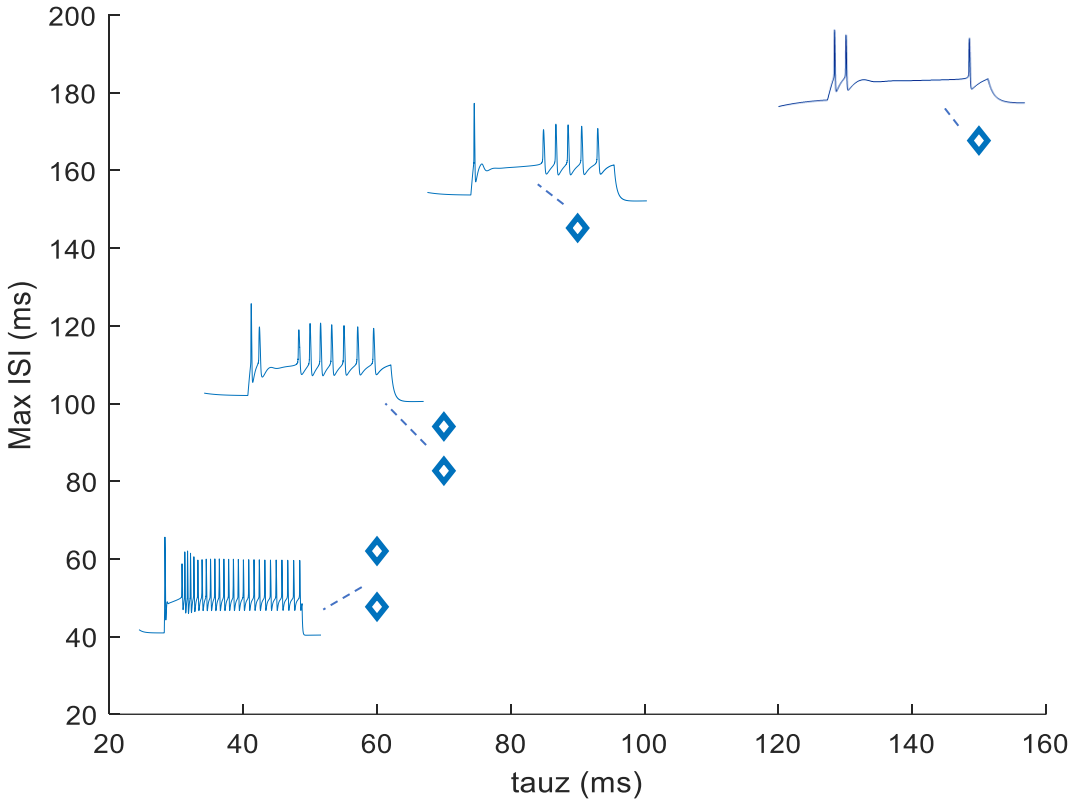

Figure 31 Variability within Type III neurons. Max ISI increases with higher values of tauz.(τ_z) The more time I_D takes to inactivate, the larger the distance separating two bursts of spikes

4.2.3 Model Confirmation: pharmacological manipulations

By fitting the diverse biological traces, we predicted the expression of the low threshold potassium currents I_M and I_D mediated by the Kv7 and Kv1 channels respectively

in HVC_{RA} neurons. These ionic predictions were confirmed in slice using specific blockers. XE991 and DTX are selective blockers for the Kv7 and Kv1 channels respectively.

Bath application of XE991 in Type I neurons (n=3) converted firing from phasic to tonic spiking (**Figure 32**). Furthermore, the model responded similarly when I_M was blocked (g_M=0 nS). Application of XE991 also resulted in a 10 mV negative shift in voltage

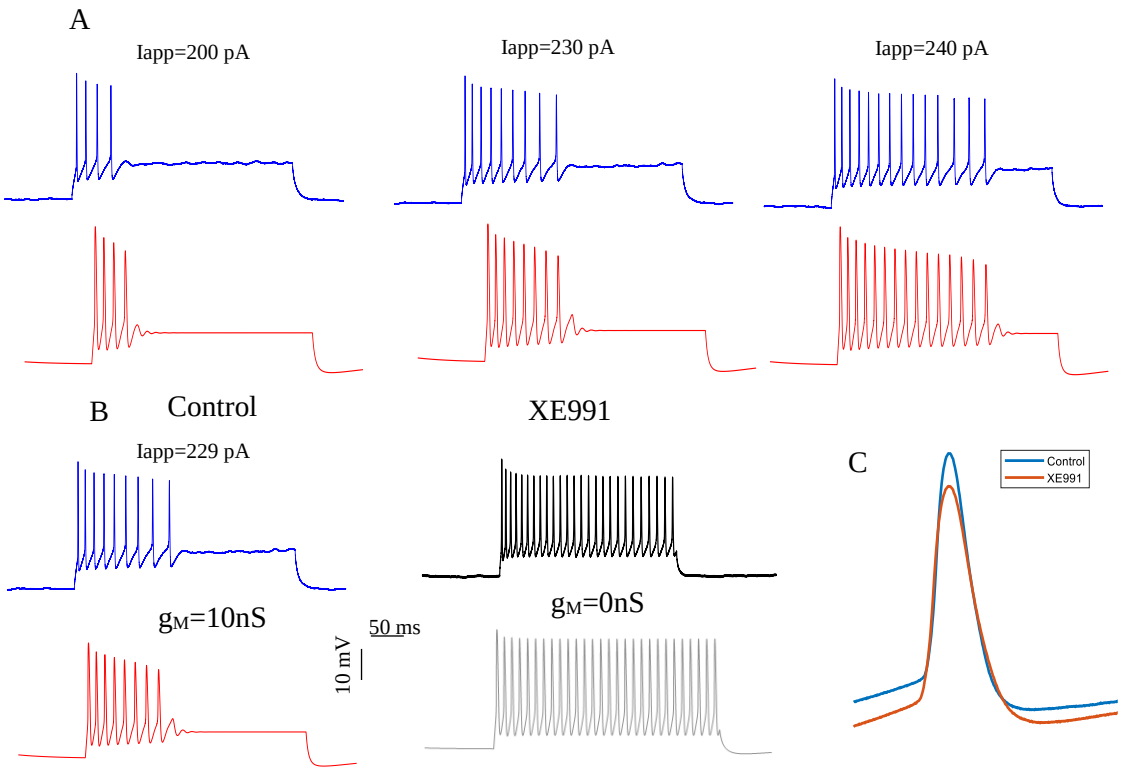

Figure 32 Expression of the M-current in type I neurons.. (A) Experimental (blue) and model (red) reposne of a type I neuron to different applied currents. (B) Bath application of XE991 converted firing from phasic to tonic. Blue and red traces correspond to the biological and modeled trace before application of XE991. Black and gray traces refer to the biological and modeled traces respectively after application of XE991. (C) First spike of the experimental traces before (blue) and after (red) XE991 application superimposed

threshold. Thus M-current mediated by the Kv7 channel is expressed in type I HVC_{RA} neurons

Bath application of DTX in type III neurons (n=2) converted firing from stuttering to tonic, negatively shifted action potential threshold by 7 mV, and reduced latency to the first spike. Similarly, the model resulted in a parallel response when I_D was blocked (g_D=0) (**Figure 33**). The resulting tonic activity after the application of DTX was characterized by adaptation which could be due to the presence of I_M and I_{SK}. Further experiments are needed to validate the presence of I_M in type III cells. Additionally, in all cases, spike width was not affected after the application of the low threshold Kv blockers indicating that both I_M and I_D do not participate in spike repolarization. Thus, preliminary pharmacological manipulations have proven the expression of both I_M and I_D in types I and III respectively.

4.2.4 Model assessment

We adopted a feature-based comparison approach to assess how well the fitted traces replicated the true biological response. Electrophysiological features of both modeled and experimental traces in response to 1.5x rheobase were evaluated (**Figure 34**). Fitted traces of the different cell types performed well in terms of firing rate, latency, firing threshold, and ISIs width. However, other features were less accurately captured by the model. Variations between modeled and experimental data arose in 1st spike amplitude, width and AHP.. The model tended to generate action potentials wider and with higher amplitudes than the experimental spikes. Therefore, the model replicated the actual neuron's response in terms

of firing rate and characteristic patterns (delay, STUT, SFA..), while more subtle features of spiking weren't accurately captured.

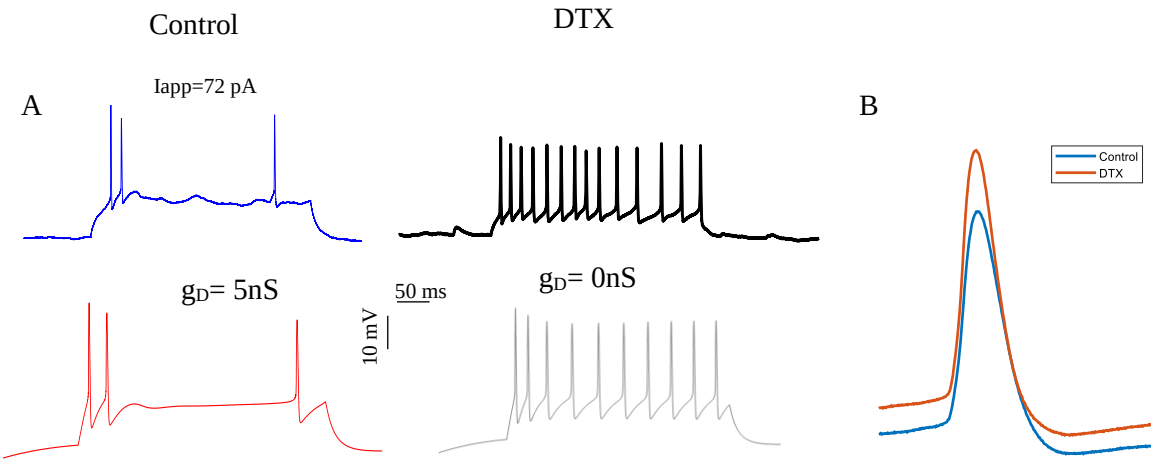

Figure 33 Expression of the D-current in type III neurons.(A) Bath application of DTX converted firing from STUT to tonic. Blue and red traces correspond to the biological and modeled trace before application of DTX. Black and gray traces refer to the biological and modeled traces respectively after application of DTX. (B) First spike of the experimental traces before (blue) and after (red) DTX application superimposed..

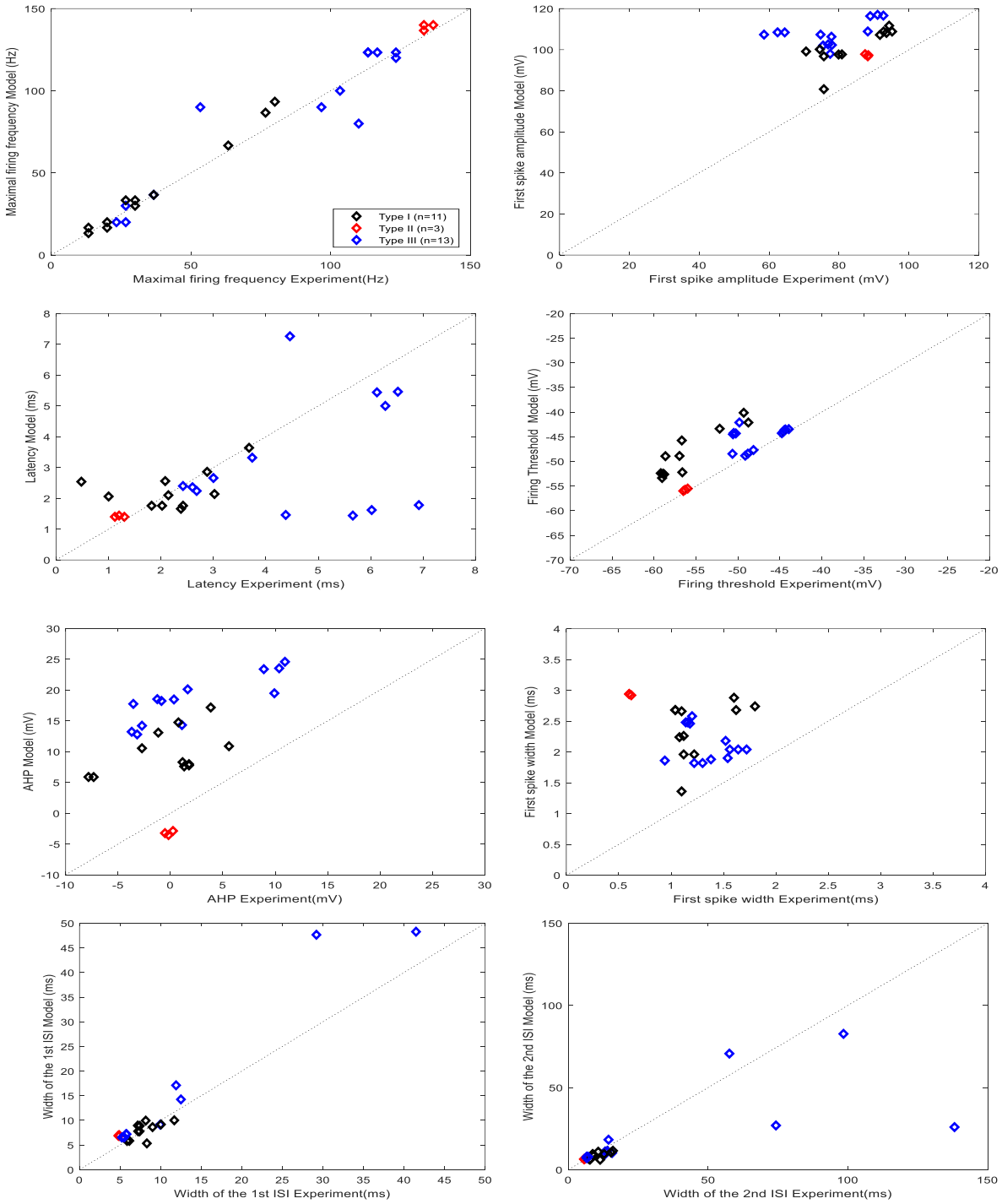

Figure 34: Comparisons between the model and experimental data for various electrophysiological features.

CHAPTER 5

DISCUSSION

In this study, we conducted a computational-based modeling approach coupled with experimental validation to characterize the electrical activity of RA-projecting neurons (HVC_{RA}) responsible for song production in zebra finches. We developed a single-compartment conductance-based model that replicated the diverse firing patterns of these neurons and predicted the presence of low thresholds potassium currents I_M and I_D driving the firing activity. These predictions were confirmed in slice using selective blockers. Revealing the underlying ionic mechanism led to a classification of these neurons based on the ion channels mainly governing their activity, suggesting that the different classes are caused by gradients of potassium currents. The novelty in this study lies first in predicting and confirming the expression of the low threshold potassium currents I_M and I_D in HVC_{RA}, and second in the model's ability to explain the diverse firing patterns and more specifically the stuttering behavior, a mechanism that wasn't thoroughly investigated previously in the literature.

While our results are the first to identify the ion channels responsible for the heterogeneity of firing within the HVC_{RA} population, a previous study by Shea and his colleagues (Shea et al. 2010) reported the existence of two types of HVC_{RA} neurons. They classified them into (i) cells that fire phasically in response to the rheobase and tonically in response to higher magnitudes of injected current, and (ii) cells only firing phasically throughout the current pulse. While there is no clear cut on classifying neurons in the nervous

system (Lourenço, Koukouli, and Bacci 2020; Markram et al. 2004), nevertheless, their findings and our current results highlight HVC_{RA}'s heterogeneity in firing, implicating that there could be diversity in the morphological and functional properties of these neurons.

Cell type classification in our study is based on either one (as in types I and II) or both (as in type III) of the low threshold potassium currents mainly governing the firing in the simulated traces (**Figure 27**), nonetheless, this does not nullify the possibility of the expression of both currents in types I and II, one current controlling the spike train and the other slightly affecting the excitability. Furthermore, our preliminary pharmacological findings confirmed the expression of Kv7 and Kv1 channels in types I and III neurons respectively (**Figure 32Figure 33**). Additional experiments are required to be conducted on a larger number of neurons to validate the existence of one or both channels in all three types and subsequently confirm the discrete or continuous classification of these neurons.

I_D and I_M mediated by Kv1 and Kv7 channels respectively, powerfully regulate the excitability in HVC_{RA} neurons. Both currents have a profound effect on firing threshold and frequency. Application of DTX and XE991 negatively shifted the firing threshold by more than 8 mV and greatly increased firing frequency. Thus, I_M and I_D, due to their activation at low thresholds, function as shunting currents around the action potential threshold effectively raising the threshold for action potential initiation and inhibiting repetitive firing.

While both currents serve to inhibit neuron's excitability and modulate action potential threshold, however, they differentially regulate the frequency–input current (FI) curve (**Figure 29**). Firing rates encode the intensity of many signals in the nervous system. For a neuron to reliably encode signals of varying intensities, it must be able to fire at low,

intermediate, and high frequencies (Drion, O'Leary, and Marder 2015). Our findings showed that I_M and I_D differentially affect HVC_{RA}'s firing rate. For example, type I neurons are characterized with slow dynamics; their firing frequency progressively increases in response to increasing step currents, while type II neurons' firing frequency increases abruptly. We showed that the progressive increase in firing rate was mainly due to the slow activation of I_M, while the sudden jump in firing frequency was due to the fast activation and very slow inactivation of I_D. Hence, I_M and I_D allow HVC_{RA} neurons to differentially filter inputs of various intensities.

Thus, the expression of Kv1 and Kv7 channels can have a significant impact on neuronal processing. In addition to regulating excitability, Kv1 channels are known to be important for controlling firing precision in neurons concerned with temporal coding in both birds and mammals (Mathews et al. 2010). They reduce input resistance and membrane time constant, thus favoring speed and precision of firing (Leão 2019). Hence, the temporally precise and sparse activity of HVC_{RA} in vivo may be associated with the expression of Kv1 channels in these neurons.

Accordingly, future studies will be necessary to unravel the actual functional roles of I_M and I_D in synchronization of the neural network. The model built could serve as a fundamental component for a larger model of the HVC network, as it incorporates the diversity of cellular properties of HVC_{RA} observed experimentally. We do note several limitations in our developed model in terms of replicating the intrinsic spiking features. The model reproduced gross features of spiking such as phasic response, long delay to firing, stuttering, and spike frequency adaptation, however, it failed to accurately capture subtle

features such as spike amplitude and width, AHP, and other (**Figure 34**). Capturing the intrinsic features of individual spikes requires tuning the kinetic properties of spike-producing currents (Na^+ and K^+). To address these limitations, an automated parameter fitting approach along with a target objective function (feature-based comparison) would be necessary to optimize the fitted model traces to the experimental data. The genetic algorithm, which is a search-based optimization technique based on the principles of genetics and natural selection., has proven to be a suitable approach for models with a large number of parameters used for fitting (Druckmann et al. 2007; Gouwens et al. 2018). The parameters set generated in this study could be implemented in this technique as an initial population to reproduce offspring (a new solution space).

CHAPTER 6

CONCLUSION

Although numerous studies attempted to characterize the HVC_{RA} electrical activity (Daou et al. 2013; Fayad 2018; Gibb et al. 2009; Jin et al. 2007), our results are the first to reproduce the diverse firing phenotypes, reveal the underlying ionic mechanism and categorize these neurons based on gradients of potassium currents.

Diversity in neuronal types is exhibited in many systems and reflects specializations necessary to encode information suited for its neurophysiological function (Leão 2019). It has been proven that intrinsic biophysical diversity assists neural coding by increasing information content (Padmanabhan and Urban 2010). Thus, the diversity within HVC_{RA} neurons reflects important specializations necessary to drive the activity in downstream areas and ultimately song production. It would be tempting to examine whether the neurons' response in area RA (innervated by HVC_{RA} neurons) is also dependent on a differential expression of ion channels in these cells. Future studies should also focus on studying the physiological relevance of the electrophysiological diversity of HVC_{RA} neurons and how this diversity would be translated into functional differences in the local neural network.

REFERENCES

Aiken, Simon P, Betty J. Lampe, and Barry S. Brown. 1995. “Reduction of Spike Frequency Adaptation and Blockade of M-current in Rat CA1 Pyramidal Neurones by Linopirdine (DuP 996), a Neurotransmitter Release Enhancer.” *British Journal of Pharmacology* 115(7):1163–68. doi: 10.1111/j.1476-5381.1995.tb15019.x.

Aiken, Simon P., Betty J. Lampe, and Barry S. Brown. 1995. “Reduction of Spike Frequency Adaptation and Blockade of M-current in Rat CA1 Pyramidal Neurones by Linopirdine (DuP 996), a Neurotransmitter Release Enhancer.” *British Journal of Pharmacology* 115(7):1163–68. doi: 10.1111/j.1476-5381.1995.tb15019.x.

Bean, Bruce P. 2007. “The Action Potential in Mammalian Central Neurons.” *Nature Reviews Neuroscience* 8(6):451–65. doi: 10.1038/nrn2148.

Berwick, Robert C., Kazuo Okanoya, Gabriel J. L. Beckers, and Johan J. Bolhuis. 2011. “Songs to Syntax: The Linguistics of Birdsong.” *Trends in Cognitive Sciences* 15(3):113–21.

Bolhuis, Johan J., Kazuo Okanoya, and Constance Scharff. 2010a. “Twitter Evolution: Converging Mechanisms in Birdsong and Human Speech.” doi: 10.1038/nrn2931.

Bolhuis, Johan J., Kazuo Okanoya, and Constance Scharff. 2010b. “Twitter Evolution: Converging Mechanisms in Birdsong and Human Speech.” *Nature Reviews Neuroscience* 11(11):747–59.

Bos, Rémi, Ronald M. Harris-Warrick, Cécile Brocard, Liliia E. Demianenko, Marin

Manuel, Daniel Zytnicki, Sergiy M. Korogod, and Frédéric Brocard. 2018. “Kv1.2 Channels Promote Nonlinear Spiking Motoneurons for Powering Up Locomotion.” *Cell Reports* 22(12):3315–27. doi: 10.1016/j.celrep.2018.02.093.

Brainard, Michael S., and Allison J. Doupe. 2002. “What Songbirds Teach Us about Learning.” *Nature* 417(6886):351–58.

Brainard, Michael S., and Allison J. Doupe. 2013. “Translating Birdsong: Songbirds as a Model for Basic and Applied Medical Research.” *Annual Review of Neuroscience* 36:489–517.

Brenowitz, Eliot A., Daniel Margoliash, and Kathy W. Nordeen. 1997. “An Introduction to Birdsong and the Avian Song System.” *Journal of Neurobiology* 33(5):495–500.

Brown, D. A., and P. R. Adams. 1980. “Muscarinic Suppression of a Novel Voltage-Sensitive K+ Current in a Vertebrate Neurone.” *Nature 1980 283:5748* 283(5748):673–76. doi: 10.1038/283673a0.

Brown, David A., and Gayle M. Passmore. 2009. “Neural KCNQ (Kv7) Channels.” *British Journal of Pharmacology* 156(8):1185–95.

Cowie, Roddy, and Ellen Douglas-Cowie. 1992. *Postlingually Acquired Deafness*. DE GRUYTER MOUTON.

Daou, Arij, and Daniel Margoliash. 2020. “Intrinsic Neuronal Properties Represent Song and Error in Zebra Finch Vocal Learning.” *Nature Communications* 11(1):1–17. doi: 10.1038/s41467-020-14738-7.

Daou, Arij, and Daniel Margoliash. 2021. “Intrinsic Plasticity and Birdsong Learning.” *Neurobiology of Learning and Memory* 180(February):107407. doi: 10.1016/j.nlm.2021.107407.

Daou, Arij, Matthew T. Ross, Frank Johnson, Richard L. Hyson, and Richard Bertram. 2013. “Electrophysiological Characterization and Computational Models of HVC Neurons in the Zebra Finch.” *Journal of Neurophysiology* 110(5):1227–45. doi: 10.1152/jn.00162.2013.

Doupe, Allison J., and Patricia K. Kuhl. 1998a. *BIRDSONG AND HUMAN SPEECH: Common Themes and Mechanisms*.

Doupe, Allison J., and Patricia K. Kuhl. 1998b. “BIRDSONG AND HUMAN SPEECH: Common Themes and Mechanisms.”

Drion, Guillaume, Timothy O’Leary, and Eve Marder. 2015. “Ion Channel Degeneracy Enables Robust and Tunable Neuronal Firing Rates.” *Proceedings of the National Academy of Sciences of the United States of America* 112(38):E5361–70. doi: 10.1073/pnas.1516400112.

Druckmann, Shaul, Yoav Banitt, Albert Gidon, Felix Schürmann, Sch¨ Schürmann, Henry Markram, and Idan Segev. 2007. *A Novel Multiple Objective Optimization Framework for Constraining Conductance-Based Neuron Models by Experimental Data*.

Dutar, Patrick, Huan M. Vu, and David J. Perkel. 1998. *Multiple Cell Types Distinguished by Physiological, Pharmacological, and Anatomic Properties in Nucleus HVc of the Adult Zebra Finch*.

Faber, E. S. Louis. 2009. “Functions and Modulation of Neuronal SK Channels.” *Cell Biochemistry and Biophysics* 55(3):127–39.

Fayad, Mira. 2018. *AN IMPROVED MODEL OF FOREBRAIN-PROJECTING CORTICAL NEURONS IN THE OSCINE SONGBIRDS*.

Fee, Michale S., and Constance Scharff. 2010. “The Songbird as a Model for the Generation and Learning of Complex Sequential Behaviors.” *ILAR Journal* 51(4):362–77. doi: 10.1093/ilar.51.4.362.

Gibb, Leif, Timothy Q. Gentner, and Henry D. I. Abarbanel. 2009. “Inhibition and Recurrent Excitation in a Computational Model of Sparse Bursting in Song Nucleus HVC.” *J Neurophysiol* 102:1748–62. doi: 10.1152/jn.00670.2007.

Giglio, Anna M., and Johan F. Storm. 2014. “Postnatal Development of Temporal Integration, Spike Timing and Spike Threshold Regulation by a Dendrotoxin-Sensitive K+ Current in Rat CA1 Hippocampal Cells.” *European Journal of Neuroscience* 39(1):12–23. doi: 10.1111/ejn.12385.

Gouwens, Nathan W., Jim Berg, David Feng, Staci A. Sorensen, Hongkui Zeng, Michael J. Hawrylycz, Christof Koch, and Anton Arkhipov. 2018. “Systematic Generation of Biophysically Detailed Models for Diverse Cortical Neuron Types.” *Nature Communications* 9(1). doi: 10.1038/s41467-017-02718-3.

Hahnloser, Richard H. R., Alexay A. Kozhevnikov, and Michale S. Fee. 2002a. “An Ultra-Sparse Code Underlies the Generation of Neural Sequences in a Songbird.” *Nature* 421(6920):294.

Hahnloser, Richard H. R., Alexay A. Kozhevnikov, and Michale S. Fee. 2002b. “An Ultra-Sparse Code Underlies the Generation of Neural Sequences in a Songbird.” *Nature* 419(6902):65–70. doi: 10.1038/nature00974.

Jarvis, Erich D. 2007. “Neural Systems for Vocal Learning in Birds and Humans: A Synopsis.” in *Journal of Ornithology*. Vol. 148.

Jin, Dezhe Z., Fethi M. Ramazanoğlu, and H. Sebastian Seung. 2007. “Intrinsic Bursting Enhances the Robustness of a Neural Network Model of Sequence Generation by Avian Brain Area HVC.” *Journal of Computational Neuroscience* 23(3):283–99. doi: 10.1007/s10827-007-0032-z.

Kalluri, Radha, Jingbing Xue, and Ruth Anne Eatock. 2019. “Ion Channels Set Spike Timing Regularity of Mammalian Vestibular Afferent Neurons.” *J Neurophysiol* 104:2034–51. doi: 10.1152/jn.00396.2010.

Kozhevnikov, Alexay A., and Michale S. Fee. 2007. “Singing-Related Activity of Identified HVC Neurons in the Zebra Finch.” *J Neurophysiol* 97:4271–83. doi: 10.1152/jn.00952.2006.

Kubota, Michinori, and Ikuo Taniguchi. 1998. *Electrophysiological Characteristics of Classes of Neuron in the HVc of the Zebra Finch*.

Kurotani, Tohru, Toshio Miyashita, Marie Wintzer, Tomokazu Konishi, Kazuhisa Sakai, Noritaka Ichinohe, and Kathleen S. Rockland. 2013. “Pyramidal Neurons in the Superficial Layers of Rat Retrosplenial Cortex Exhibit a Late-Spiking Firing Property.” *Brain Structure and Function* 218(1):239–54. doi: 10.1007/s00429-012-0398-1.

Leão, Ricardo M. 2019. “The Ion Channels and Synapses Responsible for the Physiological Diversity of Mammalian Lower Brainstem Auditory Neurons.” *Hearing Research* 376:33–46. doi: 10.1016/j.heares.2018.12.011.

Long, Michael A., Dezhe Z. Jin, and Michale S. Fee. 2010. “Support for a Synaptic Chain Model of Neuronal Sequence Generation.” *Nature* 468(7322):394–99. doi: 10.1038/nature09514.

Lourenço, Joana, Fani Koukouli, and Alberto Bacci. 2020. “Synaptic Inhibition in the Neocortex: Orchestration and Computation through Canonical Circuits and Variations on the Theme.” *Cortex* 132:258–80. doi: 10.1016/j.cortex.2020.08.015.

Markram, Henry, Maria Toledo-Rodriguez, Yun Wang, Anirudh Gupta, Gilad Silberberg, and Caizhi Wu. 2004. “Interneurons of the Neocortical Inhibitory System.” *Nature Reviews Neuroscience* 5(10):793–807.

Mateos-Aparicio, Pedro, Ricardo Murphy, and Johan F. Storm. 2014. “Complementary Functions of SK and Kv7/M Potassium Channels in Excitability Control and Synaptic Integration in Rat Hippocampal Dentate Granule Cells.” *Journal of Physiology* 592(4):669–93. doi: 10.1113/jphysiol.2013.267872.

Mathews, Paul J., Pablo E. Jercog, John Rinzel, Luisa L. Scott, and Nace L. Golding. 2010. “Control of Submillisecond Synaptic Timing in Binaural Coincidence Detectors by K v 1 Channels.” 13(5). doi: 10.1038/nn.2530.

Mooney, Richard. 2000. “Different Subthreshold Mechanisms Underlie Song Selectivity in Identified HVc Neurons of the Zebra Finch.” *Journal of Neuroscience* 20(14):5420–36.

doi: 10.1523/jneurosci.20-14-05420.2000.

Mooney, Richard. 2009. “Neural Mechanisms for Learned Birdsong.” *Learning and Memory* 16(11):655–69.

Mooney, Richard, and Jonathan F. Prather. 2005. “The HVC Microcircuit: The Synaptic Basis for Interactions between Song Motor and Vocal Plasticity Pathways.” doi: 10.1523/JNEUROSCI.3726-04.2005.

Padmanabhan, Krishnan, and Nathaniel N. Urban. 2010. “Intrinsic Biophysical Diversity Decorrelates Neuronal Firing While Increasing Information Content.” *Nature Neuroscience* 13(10):1276–82. doi: 10.1038/nn.2630.

Porter, James T., Bruno Cauli, Jochen F. Staiger, Bertrand Lambolez, Jean Rossier, and Etienne Audinat. 1998. “Properties of Bipolar VIPergic Interneurons and Their Excitation by Pyramidal Neurons in the Rat Neocortex.” *European Journal of Neuroscience* 10(12):3617–28. doi: 10.1046/j.1460-9568.1998.00367.x.

Roberts, Todd F., Sharon M. H Gobes, Malavika Murugan, Bence P. Ölveczky, and Richard Mooney. 2012. “Motor Circuits Are Required to Encode a Sensory Model for Imitative Learning.” *Nature Neuroscience*. doi: 10.1038/nn.3206.

Ross, Matthew T., Diana Flores, Richard Bertram, Frank Johnson, and Richard L. Hyson. 2017. “Neuronal Intrinsic Physiology Changes during Development of a Learned Behavior.” *ENeuro* 4(5):297–314. doi: 10.1523/ENEURO.0297-17.2017.

Rothman, Jason S., and Paul B. Manis. 2003. “The Roles Potassium Currents Play in Regulating the Electrical Activity of Ventral Cochlear Nucleus Neurons.” *J*

Neurophysiol 89:3097–3113. doi: 10.1152/jn.00127.2002.

Shah, Mala M., Michele Migliore, Ignacio Valencia, Edward C. Cooper, and David A. Brown. 2008. "Functional Significance of Axonal Kv7 Channels in Hippocampal Pyramidal Neurons." *Proceedings of the National Academy of Sciences of the United States of America* 105(22):7869–74. doi: 10.1073/pnas.0802805105.

Shea, Stephen D., Henner Koch, Daniel Baleckaitis, Jan-Marino Marino Ramirez, and Daniel Margoliash. 2010. "Neuron-Specific Cholinergic Modulation of a Forebrain Song Control Nucleus." *Journal of Neurophysiology* 103(2):733–45. doi: 10.1152/jn.00803.2009.

Shen, Weixing, Salvador Hernandez-Lopez, Tatiana Tkatch, Joshua E. Held, and D. James Surmeier. 2004. "Kv1.2-Containing K+ Channels Regulate Subthreshold Excitability of Striatal Medium Spiny Neurons." *Journal of Neurophysiology* 91(3):1337–49. doi: 10.1152/jn.00414.2003.

Shu, Yousheng, Guo Yu, Jing Yang, and David A. McCormick. 2007. "Selective Control of Cortical Axonal Spikes by a Slowly Inactivating K + Current." *Proceedings of the National Academy of Sciences of the United States of America* 104(27):11453–58. doi: 10.1073/pnas.0702041104.

Storm, Johan F. 1988. "Temporal Integration by a Slowly Inactivating K+ Current in Hippocampal Neurons." *Nature* 336(6200):698.

Storm, Johan F. 1990. "Potassium Currents in Hippocampal Pyramidal Cells." *Progress in Brain Research* 83:161–87.

Toledo-Rodriguez, Maria, Barak Blumenfeld, Caizhi Wu, Junyi Luo, Bernard Attali, Philip Goodman, and Henry Markram. 2004. “Correlation Maps Allow Neuronal Electrical Properties to Be Predicted from Single-Cell Gene Expression Profiles in Rat Neocortex.” *Cerebral Cortex* 14(12):1310–27. doi: 10.1093/cercor/bhh092.

Vu, Eric T., Mark E. Mazurek, and Yu-Chien Kuo. 1994. *Identification of a Forebrain Motor Programming Network for the Learned Song of Zebra Finches*. Vol. 14.

Wild, JM. 1993. “Descending Projections of the Songbird Nucleus Robustus Archistriatalis.” *The Journal of Comparative Neurology* 338(2):225–41. doi: 10.1002/CNE.903380207.

Yu, Albert C., and Daniel Margoliash. 1996. “Temporal Hierarchical Control of Singing in Birds.” *Science* 273(5283):1871–75. doi: 10.1126/science.273.5283.1871.

Zaika, Oleg, Lucienne S. Lara, Nikita Gamper, Donald W. Hilgemann, David B. Jaffe, and Mark S. Shapiro. 2006. “Angiotensin II Regulates Neuronal Excitability via Phosphatidylinositol 4,5-Bisphosphate-Dependent Modulation of Kv7 (M-Type) K^+ Channels.” *The Journal of Physiology* 575(1):49–67. doi: 10.1113/jphysiol.2006.114074.